Environmental Science & Technology

pubs.acs.org/est

Article

Nitrate Radicals Suppress Biogenic New Particle Formation from Monoterpene Oxidation

Dandan Li,[∠] Wei Huang,[∠] Dongyu Wang, Mingyi Wang, Joel A. Thornton, Lucía Caudillo, Birte Rörup, Ruby Marten, Wiebke Scholz, Henning Finkenzeller, Guillaume Marie, Urs Baltensperger, David M. Bell, Zoé Brasseur, Joachim Curtius, Lubna Dada, Jonathan Duplissy, Xianda Gong, Armin Hansel, Xu-Cheng He, Victoria Hofbauer, Heikki Junninen, Jordan E. Krechmer, Andreas Kürten, Houssni Lamkaddam, Katrianne Lehtipalo, Brandon Lopez, Yingge Ma, Naser G. A. Mahfouz, Hanna E. Manninen, Bernhard Mentler, Sebastien Perrier, Tuukka Petäjä, Joschka Pfeifer, Maxim Philippov, Meredith Schervish, Siegfried Schobesberger, Jiali Shen, Mihnea Surdu, Sophie Tomaz, Rainer Volkamer, Xinke Wang, Stefan K. Weber, André Welti, Douglas R. Worsnop, Yusheng Wu, Chao Yan, Marcel Zauner-Wieczorek, Markku Kulmala, Jasper Kirkby, Neil M. Donahue, Christian George, Imad El-Haddad,* Federico Bianchi,* and Matthieu Riva*

Cite This: *Environ. Sci. Technol.* 2024, 58, 1601−1614

Read Online

ACCESS | Metrics & More | Article Recommendations | Supporting Information

ABSTRACT: Highly oxygenated organic molecules (HOMs) are a major source of new particles that affect the Earth's climate. HOM production from the oxidation of volatile organic compounds (VOCs) occurs during both the day and night and can lead to new particle formation (NPF). However, NPF involving organic vapors has been reported much more often during the daytime than during nighttime. Here, we show that the nitrate radicals (NO_3), which arise predominantly at night, inhibit NPF during the oxidation of monoterpenes based on three lines of observational evidence: NPF experiments in the CLOUD (Cosmics Leaving OUtdoor Droplets) chamber at CERN (European Organization for Nuclear Research), radical chemistry experiments using an oxidation flow reactor, and field observations in a wetland that occasionally exhibits nocturnal NPF. Nitrooxy-peroxy radicals formed from NO_3 chemistry suppress the production of ultralow-volatility organic compounds (ULVOCs) responsible for biogenic NPF, which are covalently bound peroxy radical (RO_2) dimer association products. The ULVOC yield of α-pinene in the presence of NO_3 is one-fifth of that resulting from ozone chemistry alone. Even trace amounts of NO_3 radicals, at sub-parts per trillion level, suppress the NPF rate by a factor of 4. Ambient observations further confirm that when NO_3 chemistry is involved, monoterpene NPF is completely turned off. Our results explain the frequent absence of nocturnal biogenic NPF in monoterpene (α-pinene)-rich environments.

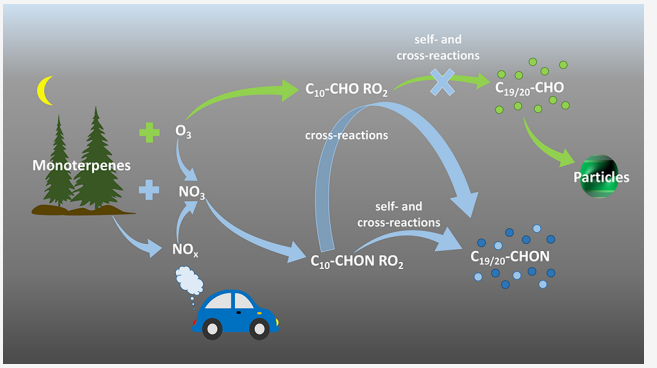

KEYWORDS: *new particle formation, gas phase chemistry, mass spectrometry, biogenic compounds*

INTRODUCTION

More than half of cloud condensation nuclei (CCN) are formed through gas-to-particle conversion of oxidation products, a process called new particle formation (NPF).[1,2] Gaseous species responsible for atmospheric NPF include sulfuric acid, nitric acid, iodine oxoacids, and highly oxygenated organic molecules (HOMs).[3−13] HOMs are formed from the gas-phase oxidation of biogenic and anthropogenic volatile organic compounds (VOCs) through multiple autoxidation reactions of peroxy radicals (RO_2).[3,5,14] It is well established that HOMs play an important role both in nucleation itself and in particle growth, either alone or by stabilizing sulfuric acid clusters.[6,15,16]

Pure organic nucleation appears to be driven by highly functionalized accretion products, which are of ultralow or

Received: September 25, 2023
Revised: November 30, 2023
Accepted: December 1, 2023
Published: January 8, 2024

extremely low volatility and are thought to be peroxides (ROOR) formed via rapid RO_2 self/cross-reactions.[6,17−20] Daytime VOC oxidation is usually initiated by reactions with hydroxyl radicals (OH) and ozone (O_3),[21,22] whereas nocturnal VOC oxidation is often initiated by nitrate radicals (NO_3) in addition to O_3.[23−25] Although ROOR are ubiquitous during both daytime and nighttime, NPF involving organic species at night is rarely reported.[7,26,27] The mechanism suppressing biogenic NPF at night remains uncertain, although it is suspected that NO_3 chemistry may play a role.[28,29] For example, it has been suggested that NO_3 oxidation of α-pinene, the most abundant monoterpene globally, is a less efficient source of secondary organic aerosol (SOA) than oxidation by either OH or O_3.[30,31] However, a recent study has shown a higher SOA yield from the α-pinene + NO_3 system depending on different RO_2 fates.[32] It is important to note that involvement in nucleation and growth is a subset of SOA formation, and therefore, it stands to reason that NO_3 oxidation might also be an inefficient source of particles. As a result, the exact role of NO_3 radicals in the formation and growth of particles remains highly uncertain.

METHODS

Kinetic and Product Characterization in the Oxidation Flow Reactor. The oxidation of α-pinene initiated by O_3 and NO_3 was conducted in an 18 L Pyrex glass oxidation flow reactor (OFR, 12 cm i.d. × 158 cm length) under dry conditions at room temperature of 296 ± 1 K and atmospheric pressure.[33] The total flow rate was kept at 16 standard liters per minute (slpm) using synthetic air (N_2/O_2 80:20), and the residence time was 67.5 s. The VOC precursor (+)-α-pinene (Sigma-Aldrich, ≥99%), O_3, and NO_2 were injected continuously using mass flow controllers (MFC, Bronkhorst). Input VOC concentration was fixed at approximately 8 ± 1 ppbv and retrieved using a quadrupole mass spectrometer (IONICON, PTR-QMS 300). NO_3 radicals were generated from the oxidation of NO_2 with O_3 in an external 1 L prereactor at atmospheric pressure and room temperature. The prereactor was dimmed to prevent the photolysis of NO_3 by room lights. 500 standard cm^3 min^{-1} (sccm) of O_2 was passed through a stable ozone generator (Fisher Scientific, SOG-1) to generate ∼900 ppbv of O_3 within the prereactor (corresponding to ∼50 ± 5 ppbv after dilution in the flow tube). O_3 was mixed with a variable NO_2 flow in the prereactor to produce different NO_3 radical concentrations. The total flow in the prereactor was fixed at 1 slpm, giving a reaction time of 60 s. Then the mixture of NO_3, O_3, and excess NO_2 entered the OFR and reacted with α-pinene. The concentrations of O_3 and NO_2 in OFR outflow (ranging from 1.9 to 75 ± 2 ppbv in the flow tube) were retrieved using a Thermo 49C and an Ecophysics CLD 88p equipped with a photolytic converter PLC 860, respectively. The particle formation was measured by a condensation particle counter (TSI CPC 3772) and remained negligible (<100 cm^{-3}) during all flow tube experiments. A chemical ionization coupled to a Q-Exactive Orbitrap mass spectrometer (CI-Orbitrap, Thermo Scientific) monitored the oxidation products.

Particle Formation in the CLOUD Chamber. New particle formation experiments were performed at CERN in the CLOUD chamber, a 3 m diameter electropolished stainless steel vessel of 26.1 m^3. This chamber enables to achieve a high standard of cleanliness and is discussed in detail by Kirkby et al.[6] The evaporation of cryogenic liquid N_2 and liquid O_2 was blended at a ratio of 79:21 to produce pure synthetic air, which constantly flushed the chamber. Variable amounts of trace gases, for example, O_3, VOCs, NO_x, SO_2, and CO, were precisely injected into the system as needed and monitored. Two hundred fifty optical fiber-optic systems installed on top of the chamber were utilized to initiate photolytic reactions, including Hg−Xe UV lamps and a UV excimer laser. The CLOUD chamber was cleaned by irrigating the walls with ultrapure water, heating to 373 K, and flushing with humidified pure air and high O_3 concentration, reducing the contaminant levels such as VOCs to less than 1 ppbv. The particles were wiped out under a high-voltage electric field. During the CLOUD 14 campaign, the total flow was kept at 250 slpm with an average residence time of 105 min. With mounting in a thermal housing, the CLOUD chamber temperature was maintained at 264 ± 0.1 K and the relative humidity at 20% for the NO_3 run. The composition inside the chamber were ceaselessly detected and analyzed by a wide range of external instruments connected to the sampling probes ∼1 m protruding into the chamber. The chamber instrumentation for the results reported here comprised an atmospheric pressure chemical ionization inlet coupled to an ultrahigh-resolution Orbitrap mass spectrometer (CI-Orbitrap, Thermo Scientific) for retrieving the chemical composition of gaseous (highly) oxygenated volatile organic compounds (OVOCs);[34] a nitrate chemical ionization atmospheric pressure interface long time-of-flight mass spectrometer (CI-(NO_3^-)-APi-LTOF, Aerodyne Research, Inc., and Tofwerk AG) from the University of Frankfurt[35] for providing the reference of HOM concentration; an iodide-adduct chemical ionization time-of-flight mass spectrometer equipped with a Filter Inlet for Gases and AEROsols (FIGAERO-CIMS, Aerodyne Research Inc.) for the composition of particles; a proton transfer reaction time-of-flight (PTR-TOF, Ionicon Analytik GmbH) mass spectrometer for organic precursor concentrations;[36] a CPC battery at 2.5−12 nm thresholds (mobility diameters); a diethylene glycol CPC (DEG-CPC) at 2.0 nm threshold;[37] a nanoscanning electrical mobility spectrometer (nSEMS) for 1.5−25 nm particle size;[38] trace gas analyzers to measure O_3 (Thermo Fisher Scientific Inc. 42i-TLE), NO (ECO Physics, CLD 780TR), and NO_2 (CAPS, Aerodyne Research Inc.); and dew point mirrors (EdgeTech) for RH of the chamber.

Field Campaign in Siikaneva, Finland. The ambient observation was conducted between March 10 and June 15, 2016, in a wetland (Siikaneva, southern Finland; 61°49′59.4"N, 24°11′32.4"E). It is located ∼5 km west of the Station for Measuring Ecosystem−Atmosphere Relations (SMEAR) II station, which is in a boreal forest at Hyytiälä. Air temperature was measured with a Rotronic HC2 sensor (Rotronic 88 AG). Global radiation was measured by a Kipp & Zonen CNR4 radiometer (OTT HydroMet B.V.). A proton transfer reaction time-of-flight mass spectrometer (PTR-TOF, Ionicon Analytik GmbH) using H_3O^+ as the ion source was used to measure the VOC concentrations. A chemical ionization atmospheric pressure interface time-of-flight mass spectrometer (CI-APi-TOF, Aerodyne Research Inc.) using NO_3^- as the reagent ion was deployed to measure the molecular composition of ambient neutral clusters. Number concentrations of particles with a mobility diameter larger than 2.5 nm were recorded with a condensation particle counter (CPC3776, TSI Inc.). The number concentration and size distribution of atmospheric ions and neutral particles with a

https://doi.org/10.1021/acs.est.3c07958
Environ. Sci. Technol. 2024, 58, 1601−1614

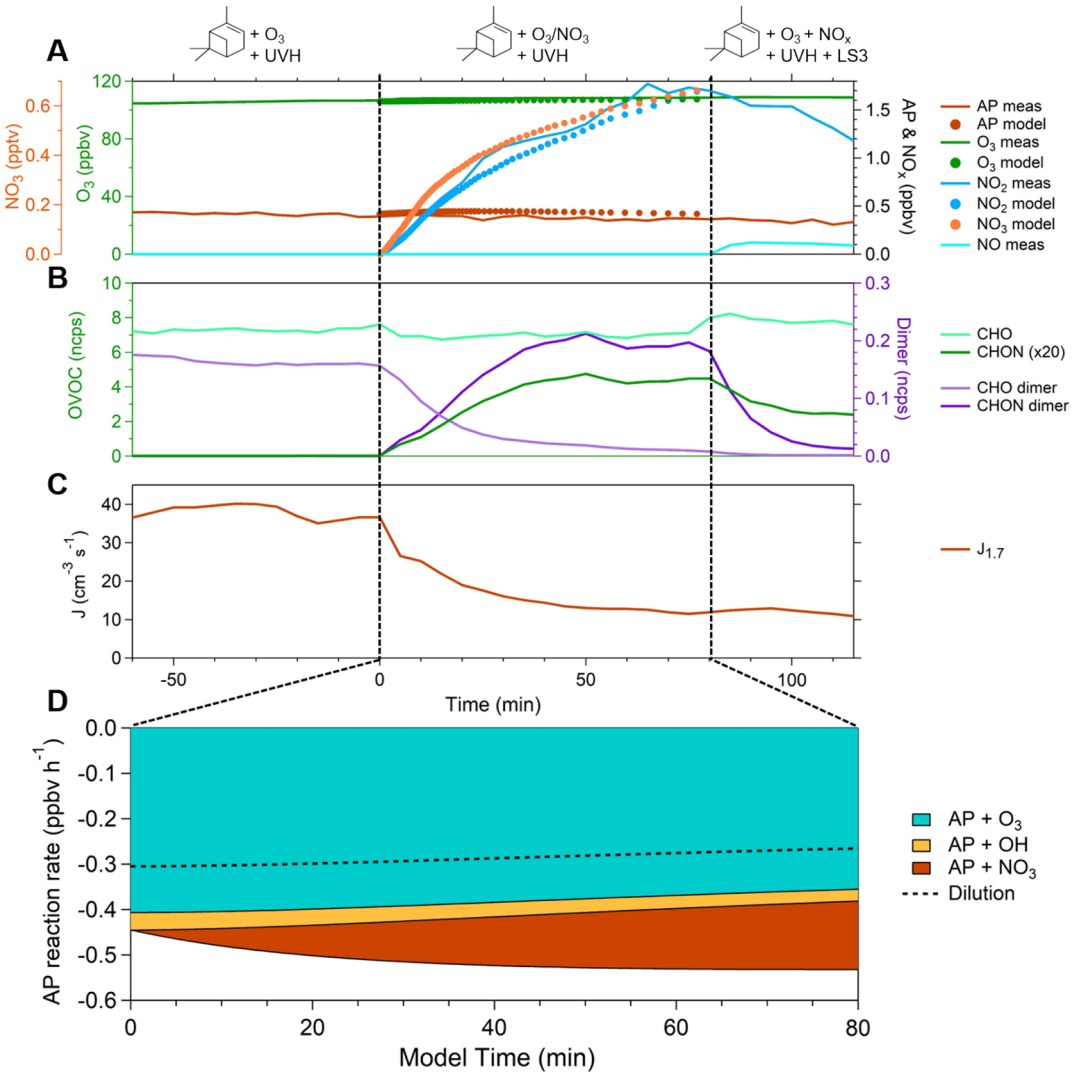

Figure 1. Effect of NO_3 radicals and NO on OVOC and particle formation in CLOUD. (A) Evolution of measured (solid line) and simulated (markers) α-pinene, O_3, NO_x, and the simulated NO_3 radical concentrations in the CLOUD chamber. Constant α-pinene (~1.3 ppb) and O_3 (~108 ppb) were injected continuously into the chamber. The experiment was conducted at 20% RH and 263 K. UVH: Hg−Xe UV lamps; LS3: LEDs were at 385 nm. When constant NO_2 (~2.5 ppb) was injected into the chamber at t = 0 min, NO_3 was generated from the reaction of NO_2 with O_3. When LS3 was turned on at t = 80 min, NO_2 was photolyzed to NO. (B) Evolution of non-nitrogen-containing total OVOCs (CHO) and dimers (CHO dimers), and nitrogen-containing total OVOCs (CHON) and dimers (CHON dimers) measured by CI-(NH_4^+)-Orbitrap. The signal of CHO dimers was multiplied by a factor of 20 for better visualization. (C) Evolution of particle formation rates (J) at 1.7 nm. (D) Evolution of the α-pinene reaction rate during the NO_3 perturbed ozonolysis stage.

mobility diameter of 0.8−42 nm were measured with a neutral cluster and air ion spectrometer (NAIS, Airel Ltd.).

Orbitrap Technology. CI-Orbitrap technology has been described elsewhere, and prior studies have reported its capabilities to study atmospheric reactive organic species successfully.[34,39] For this study, ammonium and nitrate ions (NH_4^+/NO_3^-) were used as reagent ions of CI-Orbitrap for the detection of an extensive range of OVOCs. NO_3^- ionization has been described elsewhere,[34] and NH_4^+ adduct ion chemistry has already been utilized with PTR-MS as discussed by Lindinger et al.[40] and with the novel PTR3-TOF by Hansel et al.[41] or Berndt et al.[18] and shown excellent sensitivity to detect OVOCs. Therefore, for this study, OVOCs refer to oxidized organic compounds that can be detected, including HOMs (n_O > 6) and the lower oxidized molecules (n_O = 2−5) in positive mode. NH_3 was added to the ion source taking 5 sccm from the headspace of a 1% liquid ammonium hydroxide solution (25% NH_3 basis, ACS reagent, Sigma-Aldrich). The drift in mass accuracy remained within 2 ppm throughout the experiments. The formula assignment of measured ions was constrained by known oxidation chemistry and elemental composition; i.e., ions are assumed to contain only carbon, hydrogen, oxygen, and nitrogen atoms (up to three N atoms to account for adduction of NH_4^+).

Volatility of HOMs. Because HOMs are difficult to synthesize and their vapor pressures are too low for the methods currently used to detect volatility, direct measurements of the volatilities of individual HOM are very challenging. There are numerous model calculations, such as the so-called group contribution approaches[42] or parametrizations based on the oxidation state.[43,44] We use a volatility parametrization to calculate the effective saturation mass concentration (C_{sat}) of individual organic compounds according to their structure-based estimations and formula-

https://doi.org/10.1021/acs.est.3c07958
Environ. Sci. Technol. 2024, 58, 1601−1614

based estimations using the modified Li et al. approach[44] as in eq 1:

$$\log_{10}C_{sat}(298\ \mathrm{K}) = (n_C^0 - n_C)b_C - n_O b_O - 2\frac{n_C n_O}{(n_C + n_O)}b_{CO} - n_N b_N - n_S b_S \quad (1)$$

where n_C, n_O, n_N, and n_S are the number of carbon, oxygen, nitrogen, and sulfur atoms of the specific molecule, separately; n_C^0 is the reference carbon number; b_C, b_O, b_N, and b_S are the contribution of each atom to $\log_{10}C_{sat}$ separately; and b_{CO} is the carbon−oxygen nonideality. Values of the b coefficient can be found in Li et al.[44] The formula used to estimate the vapor pressure is amended to convert all NO_3 groups into OH groups to reduce the bias from the compounds containing nitrates.[45,46]

Because of the different temperatures in the CLOUD 14 experiments, we adjusted the C_{sat}(298 K) to the measured experimental temperature in eqs 2 and 3:

$$\log_{10}C_{sat}(T) = \log_{10}C_{sat}(298\ \mathrm{K}) + \frac{\Delta H_{vap}}{R\ln(10)} \times \left(\frac{1}{298} - \frac{1}{T}\right) \quad (2)$$

$$\Delta H_{vap}(\mathrm{kJ\ mol^{-1}}) = -11 \cdot \log_{10}C_{sat}(298\ \mathrm{K}) + 129 \quad (3)$$

where T is the temperature in kelvin, C_{sat}(298 K) is the saturation mass concentration at 298 K, ΔH_{vap} is the evaporation enthalpy, and R is the gas constant (8.3134 J K^{-1} mol^{-1}). The potential presence of isomers may result in uncertainty in this method because the only input is a molecular formula.

In this study, all oxidation products were grouped into six volatility regimes based on VBS—ultralow volatility (ULVOCs), $C_{sat} < 10^{-8.5}$ $\mu g\ m^{-3}$; extremely low volatility (ELVOCs), $10^{-8.5} < C_{sat} < 10^{-4.5}$ $\mu g\ m^{-3}$; low volatility (LVOCs), $10^{-4.5} < C_{sat} < 10^{-0.5}$ $\mu g\ m^{-3}$; semivolatile (SVOCs), $10^{-0.5} < C_{sat} < 10^{2.5}$ $\mu g\ m^{-3}$; intermediate volatility (IVOCs), $10^{2.5} < C_{sat} < 10^{6.5}$ $\mu g\ m^{-3}$; and VOCs, $10^{6.5} < C_{sat}$ $\mu g\ m^{-3}$.

Kinetic Model Simulations. The behaviors of NO_3, N_2O_5, and RO_2 ($C_{10}H_{15}O_4$, $C_{10}H_{17}O_3$, and $C_{10}H_{16}NO_5$), and the corresponding less oxidized monomers formed from the oxidation reaction of α-pinene by O_3/OH and NO_3 radicals were simulated simply using the F0AM v3.1[47] box model employing MCM v3.3.1.[48] The RO_2 autoxidation reactions and NO_3 chemistry-related packages were not considered in the model.

RESULTS

Here we examine the reactivity of α-pinene with varying levels of NO_3 radicals and the influence of different HOM compositions on NPF. We draw on three data sets: experiments conducted in the CLOUD chamber at CERN, laboratory OFR experiments, and field measurements in a wetland surrounded by boreal forests (Siikaneva, Finland) (see Methods for experimental details). Controlled laboratory experiments were performed using α-pinene, as it is one of the most abundant biogenic VOCs in the atmosphere[49] and one of the key precursors to produce HOMs.[6]

NPF with Different Oxidants. Figure 1 shows the evolution of reactant and reaction product concentrations together with the resulting particle formation rates measured in the CLOUD chamber. We broke the experiment into three stages to examine different radical chemistry under otherwise identical conditions, including approximately 1000 ppbv of carbon monoxide to scavenge the OH radicals formed from the ozonolysis of α-pinene and homogeneous illumination from four Hg−Xe arc lamps (UVH, Figure S1). We first examined the reaction of α-pinene with O_3. At t = 0 min, NO_2 was continuously injected into the chamber to form NO_3. The production rate of NO_3 was 0.3 ppbv h^{-1}, similar to that observed in the atmosphere, and the NO_3 concentration was estimated using the 0-D box model (F0AM).[47] Finally, at t = 80 min, LEDs at 385 nm (LS3) were switched on to form NO via NO_2 photolysis and convert NO_3 into NO_2. The three conditions were thus pure ozonolysis, ozonolysis perturbed by NO_3, and ozonolysis perturbed by NO. Although NO_2 might play a role during stage 3, a larger concentration of nitrogen containing species (Figure S3) indicates that NO has a major role in perturbing RO_2 chemistry.

Non-nitrogen-containing OVOCs (CHO) formed through the ozonolysis of α-pinene comprise monomers $C_{9,10}H_{12,14,16,18}O_{\geq 2}$ (CHO monomers) and dimers $C_{19,20}H_{28,30,32}O_{\geq 4}$ (CHO dimers), which predominated during its ozonolysis. NO_2 injection and NO_3 formation resulted in a sharp decrease in the concentrations of the CHO dimers (Figure 1B). At the end of the second stage, CHO dimer formation was significantly reduced as NO_3 radicals rose toward a concentration of only 0.6 pptv even though measured O_3 and α-pinene concentrations remained constant (Figure 1A). Meanwhile, we observed a large formation of nitrogen-containing species (CHON), including monomers $C_{9,10}H_{13,15,17}O_{\geq 4}N$ (CHON monomers) and two classes of dimers (CHON dimers): $C_{19,20}H_{29,31,33}O_{\geq 5}N$ ($CHON_1$ dimers) and $C_{20}H_{32}O_{\geq 8}N_2$ ($CHON_2$ dimers), with the concentrations of CHON dimers being higher than those of CHO dimers during pure ozonolysis (~1.4-fold) (Figure 1B). Good agreement between NH_4^+-Orbitrap and NO_3^--LTOF (a nitrate CI atmospheric pressure interface long time-of-flight mass spectrometer)[39] for the detection of CHO and CHON species indicates similar sensitivity for the different mass spectrometers (Figure S2).

Added NO_3 increased the overall concentration of dimers due to the greater formation of CHON dimers. During this stark change in dimer composition, the net formation rate of particles at 1.7 nm ($J_{1.7}$) decreased by a factor of 4, implying that the NO_3 chemistry strongly suppresses α-pinene NPF (Figure 1C). After the lights were switched on at t = 80 min, the NO_3 radicals were scavenged mainly by reaction with NO as well as by photolysis; subsequently, oxidation proceeded via ozonolysis under high NO_x conditions. The presence of NO_x terminated the bimolecular reactions of RO_2 generated from the O_3 + α-pinene (CHO RO_2) and formed CHON monomers (Figures 1B and S3), whereas the formation pathway of CHON dimers was cut off as a result of the absence of nitrooxy peroxy radicals, which are generated from the NO_3 radical addition to α-pinene (CHON RO_2). As Figure 1C shows, the particle formation rates did not change even at higher CHO concentrations when the lights were turned on, which is consistent with previously observed lower J values at higher NO_x, where NO_x terminates the formation of dimers by controlling the branching reactions of RO_2 radicals.[50] This indicates that NO_3 chemistry suppresses particle formation to a similar extent as NO does[50] even though NO_3-initiated

https://doi.org/10.1021/acs.est.3c07958
Environ. Sci. Technol. 2024, 58, 1601−1614

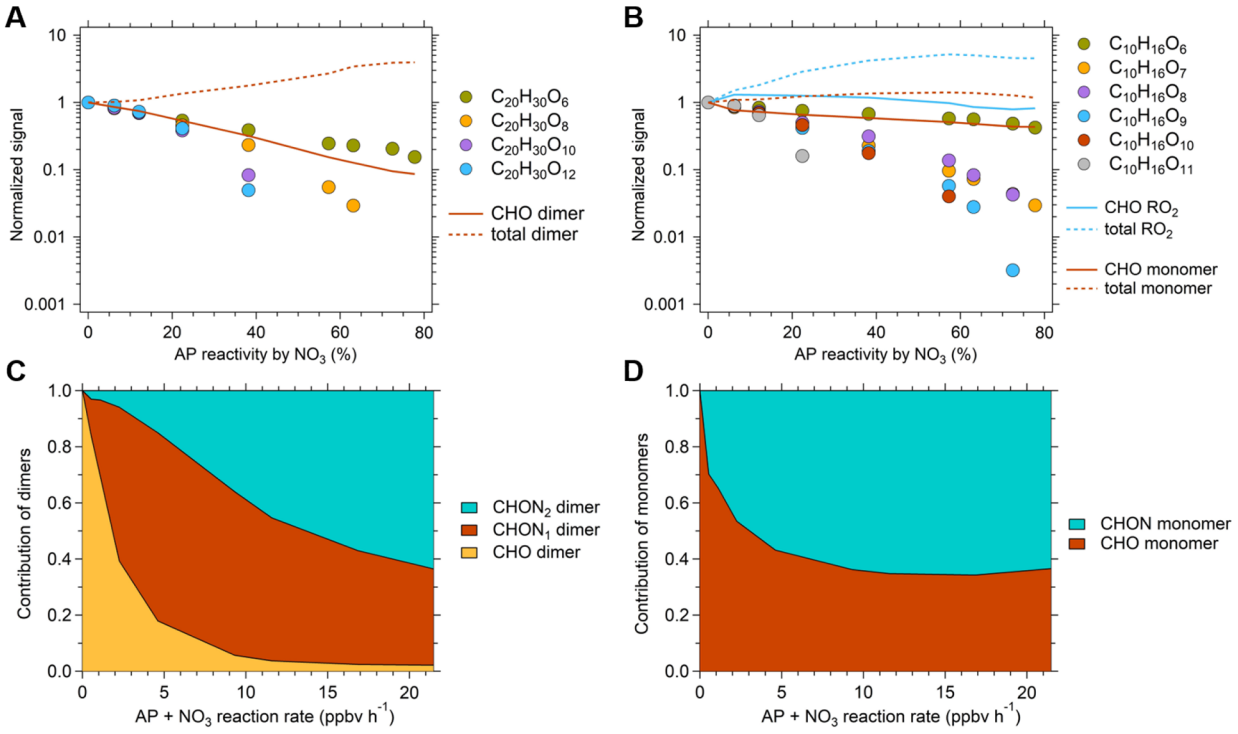

Figure 2. Sensitivity of NO_3 radicals to the formation of OVOCs in an oxidation flow reactor. (A, B) Normalized signals of non-N-containing dimers (CHO dimers) and total dimers (total dimers) (A), non-N-containing monomers (CHO monomers), total monomers (total monomers), non-N-containing RO_2 radicals (CHO RO_2), and total RO_2 radicals (total RO_2) (B) as a function of α-pinene reactivity by NO_3 radicals measured by CI-(NH_4^+)-Orbitrap in oxidation flow reactor (OFR) experiments. Ion signals are normalized to the signal in the O_3/OH chemistry for comparison. A missing data point indicates that the signal intensity is below the detection limit of the instrument (10^5 molecules cm^{-3}). Experiments were conducted at ~8 ppbv α-pinene, ~ 50 ppbv O_3, 296 K, and RH < 1%. Nine different NO_2 concentrations were injected varying from 0 to 75 ppbv in a flow tube. Every point represents the steady-state concentrations of products. (C, D) Contribution of non-N-containing dimers (CHO dimers), 1-N-containing dimers ($CHON_1$ dimers), and 2-N-containing dimers ($CHON_2$ dimers) to total dimers (C) and non-N-containing monomers (CHO monomers) and N-containing monomers (CHON monomers) to total monomers (D) plotted against the α-pinene oxidation rate by NO_3 radicals.

oxidation of α-pinene yields a large concentration of dimeric compounds, unlike NO.

The evolution of the α-pinene reaction in the NO_3 chemistry stage is shown in Figure 1D. The same amount of α-pinene reacted with O_3 in the presence of NO_3 radicals, whereas the total reacted α-pinene increased by 10%. NO_3 chemistry suppression of NPF occurred even though most of the α-pinene oxidation was still driven by O_3 (Figure 1D and Figure S4) and even though the overall concentration of dimers produced with NO_3 present was substantially higher than that during the pure ozonolysis.[51] Our F0AM simulations show that almost all CHO RO_2 radicals predominantly undergo self/cross-reactions and reactions with the HO_2 pathway, indicating that the presence of NO_3 and NO_x did not fundamentally modify the dimer branching ratios of RO_2 radicals (Figure S5). The results suggest that CHON RO_2 produced from NO_3 oxidation are highly reactive and dimers formed through NO_3 chemistry must be significantly more volatile than dimers formed from O_3 chemistry. This is similar to isoprene suppression of biogenic NPF where the resulting oxidation products (i.e., C_{14}–C_{15} dimers) are more volatile than those from monoterpenes alone.[52,53] Importantly, the sharp decrease in particle formation rates occurred at very low NO_3 concentrations relative to those of O_3 even though the reaction with O_3 remained the dominant α-pinene oxidation process (Figure 1D and Figure S4). Thus, NO_3 chemistry fundamentally alters the product distributions and volatility even when it represents only a small fraction of the total α-pinene reactivity, i.e., less than 30% (Figure S4).

HOM Distribution at Different NO_3 Levels. To further investigate the influence of different steady-state concentrations of NO_3 radicals on α-pinene oxidation, we performed extensive OFR experiments in the presence of O_3, OH, and NO_3 radicals. In addition to an experiment without any NO_2 addition, we also investigated eight NO_2 to O_3 ratios between 0.03:1 (close to the ratio of 0.023:1 for the CLOUD experiments) and 1.5:1 (Figure S6). Over this range, no NPF occurred because of the short residence time inside OFR, and the simulation shows that the rate of the α-pinene reaction with O_3 remained constant, but the total α-pinene reactivity increased by a factor of 3 relative to that in the O_3/OH chemistry (Figure S7a). Ultimately up to ~80% of the α-pinene loss was from NO_3 oxidation at the highest NO_2/O_3. Meanwhile, the fraction of α-pinene oxidized by OH radicals decreased from 44% to 6% because NO_2 scavenged the OH. Similarly, other than the reaction with NO_2 (resulting in approximately 50 to 2000 pptv of N_2O_5 in the OFR), NO_3 radicals were almost completely consumed by α-pinene, and the reactions of CHO RO_2 + NO_3 and CHO RO_2 + NO_2 did not play a significant role in modifying the product distribution (Figure S8).

Like the CLOUD observations, the presence of NO_3 radicals fundamentally alters the product distribution (Figure S9). All CHON dimers identified in the CLOUD chamber were found

https://doi.org/10.1021/acs.est.3c07958
Environ. Sci. Technol. 2024, 58, 1601−1614

in OFR, but more CHON monomers and OH-initiated species were observed in OFR due to its short residence time and the absence of an OH scavenger (Figure S10). Figure 2 shows the sensitivity of oxidation products generated from α-pinene and the fraction reacting with NO_3 vs O_3/OH. Specifically, at maximal NO_3 concentrations, CHO dimers' intensity is ~10 times lower compared to experiments performed without NO_3 (Figure 2A). CHO monomers are much less sensitive to the increasing level of NO_3 radicals in α-pinene oxidation, with only a 2.3-fold decrease, which is probably due to the cross-reactions of CHO RO_2 and CHON RO_2. This is consistent with our F0AM simulation, which shows a 1.4-fold decrease for the less oxidized CHO monomer (i.e., n_O = 2−5) concentrations (Figure S11). However, the sharper reduction of the most oxidized CHO (i.e., n_O > 6) as the NO_3 contribution increases (up to a 10-fold decrease) indicates that the suppression of ozonolysis products by NO_3 is most important for the most highly oxygenated monomer and dimer products (Figures 2 and S12).

In contrast to CHO dimers (10-fold decrease), the concentrations of products identified as CHO RO_2 (with an odd number of H atoms, including $C_{10}H_{15}O_{4-10}$ and $C_{10}H_{17}O_{3-7}$) do not differ much in the presence of NO_3 versus O_3/OH chemistry, with slight fluctuations across all different NO_3 reactivities (Figure 2B). In contrast to a 20% reduction in simulated $C_{10}H_{15}O_x$ radicals, the measured $C_{10}H_{15}O_x$ rose with NO_3 radicals, likely as a result of the additional $C_{10}H_{15}O_x$ produced by the H-abstraction pathway from the reaction of NO_3 radicals with α-pinene that was not included in the model (Figures S11, S12e, and S13). Concentrations of $C_{10}H_{17}O_{5,7}$ radicals from OH chemistry decreased by a factor of 9 because of the lowered reactivity of α-pinene with OH and more loss via bimolecular reactions (Figures S7 and S12f). CHON RO_2 (including $C_{10}H_{16}O_{5,6,7,9}N$) started to play an important or even dominant role as soon as NO_3 radicals were produced (Figures S13 and S14e).

Unlike the case for the O_3/OH chemistry, the NO_3 chemistry yields a solitary RO_2 species (i.e., $C_{10}H_{16}NO_5$), the autoxidation of which is very limited. This is shown by comparing the signal of a "parent" RO_2 to its more oxygenated autoxidation products (Figure S13). Although uncertainties remained in the quantification of RO_2 radical concentrations, chemical ionizations were reported to exhibit the same sensitivity for the O_3-derived RO_2 radicals,[54] and NH_4^+-Orbitrap did not show any distinct sensitivity to CHON species compared to CHO species (Figure S2). The average ratio of $C_{10}H_{15}O_4$ to ($C_{10}H_{15}O_6$ + $C_{10}H_{15}O_8$), which are ozonolysis products, was 4.0 ± 0.3. In contrast, the ratio of $C_{10}H_{16}NO_5$ to ($C_{10}H_{16}NO_7$ + $C_{10}H_{16}NO_9$), from NO_3 oxidation, was 72 ± 14 (Figure S13). Such a large difference is likely caused by the ring-retaining structure of $C_{10}H_{16}NO_5$ preventing the H-shift isomerization involved in the autoxidation of peroxy radicals.[54,55] The concentrations of CHON RO_2, $CHON_1$ dimers, and CHON monomers seemed to be constant when the α-pinene reactivity by NO_3 reached ~40%, indicating that newly formed CHON RO_2 proceed immediately via a propagation cycle to form RO radicals or via an accretion reaction to form $CHON_2$ dimers at higher NO_3 levels (Figure S14).

The contribution to total dimers of $CHON_1$ dimers generated from the cross-reaction between CHON RO_2 and CHO RO_2 increased with an increasing contribution of NO_3 to α-pinene reactivity and peaked (67%) when the α-pinene reaction rate with NO_3 radicals was greater than 5 ppbv h^{-1}, corresponding to ~40% of total α-pinene reactivity, after which its dominance was gradually replaced by $CHON_2$ dimers produced from CHON RO_2 self/cross-reactions (Figure 2C and Figure S7). The proportion of CHON monomers to total monomers also reached its highest value (60%) at this α-pinene reaction rate (i.e., 5 ppbv h^{-1}) and then remained constant (Figure 2D). Results obtained with the CI-Orbitrap operated in negative mode (NO_3^-) further support the role of CHON RO_2 in the distribution of OVOCs (Figure S15). However, it should be mentioned that the nitrate reagent ion is selective toward HOMs, i.e., n_O > 6 for CHO monomers and n_O > 8 for CHON monomers, which explains the general decreasing trend of OVOCs (i.e., monomers and dimers) measured by the CI-(NO_3^-)-Orbitrap. Overall, the OFR results indicate that the presence of CHON RO_2 competes against autoxidation and CHO dimer formation, two mechanisms responsible for monoterpene NPF, resulting in a net reduction of CHO species formed from O_3/OH oxidation.

Change of HOM Volatility Distribution by NO_3. Higher volatilities of CHON dimers than CHO dimers in the particle phase are confirmed by thermal desorption measurements performed by a FIGAERO-CIMS[56] (Figure 3A). It is worth mentioning that unlike monomers, thermal fragmentation contributions are negligible for larger compounds like dimers during particle desorption within the FIGAERO.[57,58] The maximum desorption temperatures (T_{max}) of particulate CHON dimers were much lower (40−85 °C) than T_{max} of particulate CHO dimers (~110 °C), corresponding to saturation vapor concentrations (C_{sat}) of 10^{-3} to 10^{1} $\mu g\ m^{-3}$ for CHON dimers and 10^{-5} to 10^{-7} $\mu g\ m^{-3}$ for CHO dimers.[59] The saturation vapor concentrations of particulate OVOCs in the CLOUD chamber experiments are predicted using the VBS parameterizations.[60,61] Parameterized $\log_{10}C_{sat}$ agree well with the measured $\log_{10}C_{sat}$ for particulate CHO species (Figure S16a). In addition, measured $\log_{10}C_{sat}$ of particulate dimers show a good correlation (R^2 = 0.85) with their estimated $\log_{10}C_{sat}$ using the modified Li et al. approach[44] accounting for nitrate functionalities (Figure S16b).

Therefore, we estimated the volatility distribution of the full-range OVOCs measured by CI-(NH_4^+)-Orbitrap in the CLOUD chamber (Figure 3B and Figures S17 and S18) using the modified Li et al. approach.[44] As shown in Figure 3B, we grouped monomers C_{9-10} and dimers C_{18-20} measured in the CLOUD chamber into five volatility regimes based on their $\log_{10}C_{sat}$ values:[61,62] ultralow-volatility (ULVOCs), extremely low-volatility (ELVOCs), low-volatility (LVOCs), semivolatile (SVOCs), and intermediate-volatility (IVOCs) organic compounds. Only the ULVOCs and some ELVOCs initiate cluster growth and form new particles.[61,63] In each volatility bin, we show the signal of the sum of OVOCs that fall in this volatility range. Because of the negligible CHON RO_2 autoxidation, the volatility distribution of OVOCs shifts toward relatively higher volatility in the presence of NO_3 radicals compared to the distribution from pure O_3 chemistry (Figure 3B). The resulting average signal weighted C_{sat} value is 2 times higher in the presence of NO_3 radicals. However, the effect is most dramatic in the tail for compounds directly involved in NPF. The contribution of ELVOCs drops by a factor of 2 (i.e., from 1.7 to 0.8%), and the ULVOCs, which contribute most efficiently to pure biogenic nucleation,[63] comprise 0.6% of the total measured OVOCs in the pure O_3 system but decrease to 0.1%

https://doi.org/10.1021/acs.est.3c07958
Environ. Sci. Technol. 2024, 58, 1601−1614

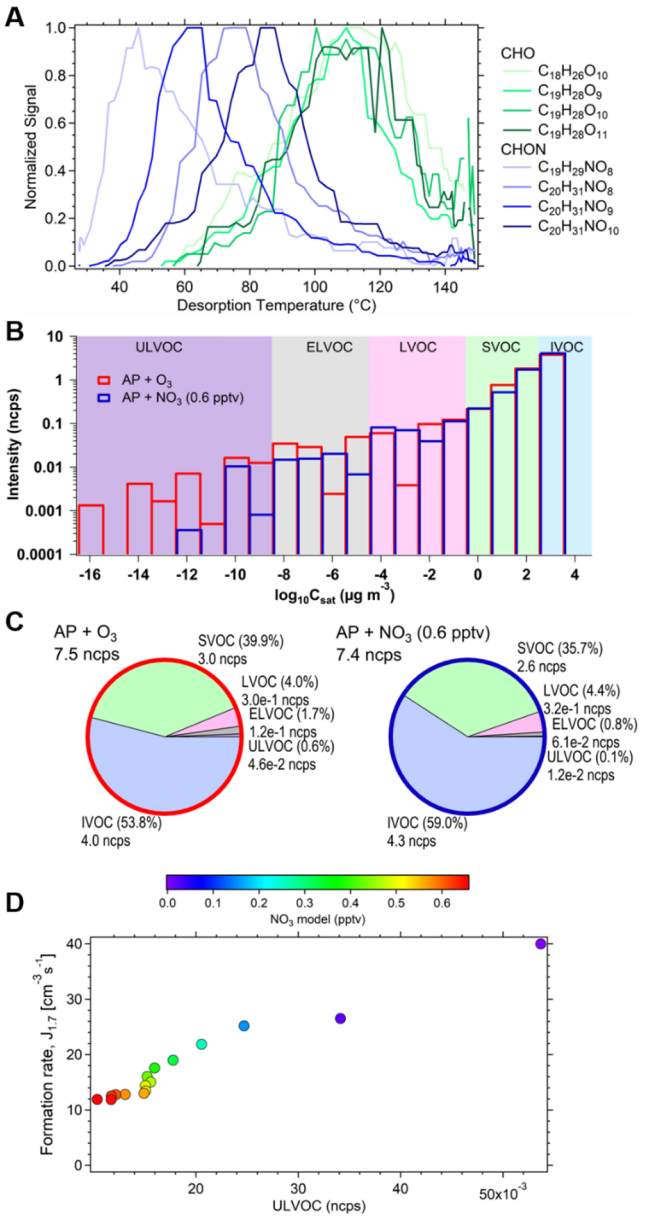

Figure 3. Higher volatilities of OVOCs in the presence of NO_3 radicals illustrating the suppression of NPF in CLOUD. (A) Desorption signals of the most abundant CHO dimers and CHON dimers in the particle phase measured by FIGAERO-CIMS. Ion signals are normalized to the maximum signal on a linear scale for clarity. (B) Monomers C_{9-10} and dimers C_{18-20} measured by CI-(NH_4^+)-Orbitrap binned to a volatility distribution showing their relative abundance in pure O_3 and NO_3 chemistry, respectively; the simulated NO_3 concentration was ~0.6 pptv. The background colors represent the saturation concentration (C_{sat}) in the range of ultralow-volatility (ULVOCs, purple), extremely low volatility (ELVOCs, gray), low-volatility (LVOCs, pink), semivolatile (SVOCs, green), and intermediate-volatility (IVOCs, blue) organic compounds. (C) Corresponding contributions of IVOC, SVOC, LVOC, ELVOC, and ULVOC classes in pure O_3 and NO_3 chemistry. These percentages do not relate to the yields but to the measured intensities. (D) Formation rate of particles plotted as a function of ULVOC concentration colored by the concentrations of simulated NO_3 radicals.

in the presence of NO_3 radicals (Figure 3C). The lowest volatility bins of the ULVOC range ($log_{10}C_{sat} < -13$ μg m^{-3}) vanish entirely. A 5-fold reduction of the ULVOC yield was also quantified using the NO_3^--LTOF.

As the OVOC composition changed during the experiment, the decrease of the measured particle formation rates at 1.7 nm by a factor of 4 (see also Figure 1C) is likely driven by the decreasing concentration of ULVOCs caused by an increase in the NO_3 radical concentration, although the α-pinene O_3 reactivity remained constant (Figures 1D and 3D). Overall, the results demonstrate that NO_3 radicals inhibit the production of the least volatile compounds and ultimately inhibit the formation of new particles.

Nocturnal NPF in a Wetland. We further investigated the role of NO_3 radicals in suppressing NPF from the ozonolysis of monoterpenes by conducting night-time observations in a wetland surrounded by boreal forests in Siikaneva, Finland. At this location, we did observe rare nocturnal NPF events (Figure S19), which were found to be accompanied by a decoupled layer formation capturing the emissions from the wetland inside this stable surface layer and nearly no mixing with the rest of the atmosphere.[64] More details for the characteristics of these nocturnal NPF events can be found in Junninen et al.[65] Sulfuric acid concentrations were found to be similar for event night (below 1.8×10^5 molecules cm^{-3}) and nonevent night (below 2.2×10^5 molecules cm^{-3}, Figure S20), suggesting that H_2SO_4 cannot explain the difference of nocturnal NPF observed in Siikaneva. Similar OVOC species as in the CLOUD chamber were detected in this ambient environment (Figure S21). Monoterpenes were found to be the dominating VOCs at this site (Figure S20), and the most abundant monoterpene species there were found to be α-pinene and Δ^3-carene.[66] These species were thus used to calculate the reactivity of different monoterpene isomers in the wetland to represent the reactivity range in Siikaneva by assuming the total monoterpene concentration is that of one monoterpene. The resulting reactivity of ozonolysis with these two monoterpenes and the generated concentrations of CHO dimer were on average 3 times and 2 times higher during the nighttime NPF event compared to nonevent night, respectively, with the dominating monoterpene ozonolysis reactivity in Siikaneva from α-pinene (Figures 4 and S22a). Further, concentrations of the CHO monomer and CHO dimer were 4 and 10 times higher than those of the CHON monomer and CHON dimer during the NPF event, respectively, with total CHO species representing 80% of total OVOCs. In contrast, sharp increases of CHON monomer and CHON dimer were observed only during the nonevent when no decoupling process occurred but in well-mixed conditions with the rest of the atmosphere.[64] The presence of CHON dimers, which are markers for NO_3 chemistry, indicates the presence of NO_3 during the nonevent night,[29,64] which was estimated at nearly 1 ppqv, resulting in a reactivity of monoterpene of 0.2 pptv h^{-1} during the nonevent night ($NO_2/O_3 \approx 0.007{:}1$), with the reactivity of monoterpenes by NO_3 radicals in Siikaneva mainly coming from α-pinene (Figure S22b). These were associated with a corresponding drop in ULVOC and ELVOC concentration by a factor of 6 (Figure 4G). Consistent with the CLOUD experiments, the particle number concentration is up to 1 order of magnitude (3-fold in median) lower during the nonevent night compared to event night (Figure 4A).

Taken together, these results form the basis of a molecular understanding of why biogenic NPF is not commonly observed at night, especially in α-pinene-dominated environments. The NO_3-derived RO_2 radicals formed from α-pinene oxidations

https://doi.org/10.1021/acs.est.3c07958
Environ. Sci. Technol. 2024, 58, 1601−1614

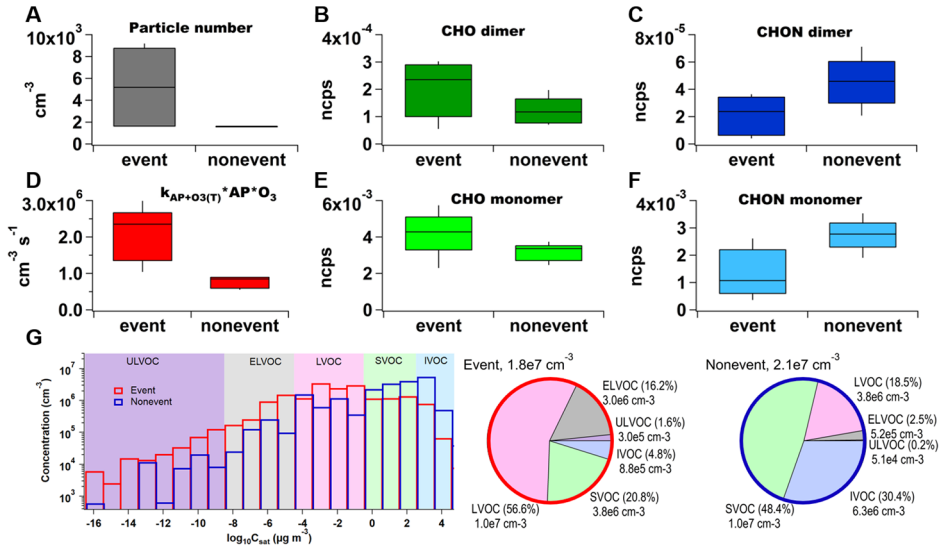

Figure 4. Nocturnal NPF event and nonevent recorded at Siikaneva, Finland. (A–F) Box plots of number concentrations of particles greater than 2.5 nm (A), CHO dimers (B), CHON dimers (C), α-pinene ozonolysis rate (D), CHO monomers (E), and CHON monomers (F) in one NPF event and one nonevent. (G) Binned volatility distribution of monomers C_{9-10} and dimers C_{19-20} measured by CI-(NO_3^-)-APi-TOF showing their concentration for a NPF event and a nonevent. The pie charts on the right represent the corresponding contributions of IVOC, SVOC, LVOC, ELVOC, and ULVOC classes.

not only yield higher volatility dimers but also completely alter the fate of RO_2 radicals from other oxidants and thus their capacity to form new particles. The nitrogen-containing organic vapors formed from the NO_3 chemistry are not of sufficiently low volatility to initiate the formation and growth of particles. When only 20–30% of the α-pinene reactivity is driven by NO_3, ULVOC yields are reduced by a factor of 5 and particle formation rates by a factor of 4. In the ambient atmosphere, the particle number is cut by up to an order of magnitude in α-pinene-dominated environments when NO_3 chemistry is involved. In general, the quantity and volatility distribution of HOMs, HOM-RO_2, and RO_2 produced from concurrent complex chemical reactions can substantially alter the formation of new particles in the atmosphere. This is especially important for organic NPF governed by covalently bound dimers, where cross-reactions between different RO_2 control the ULVOC tail of the volatility distribution and exact NPF rates depend even on the volatility distribution within that tail. In some cases, such as for isoprene suppression of monoterpene nucleation, it is the mixture of organic precursors that influences the outcome.[52,53] In others, such as for NO_x suppression, it is the inhibition of dimer formation that affects the outcome.[50] Here, for NO_3 suppression, it is the oxidant that influences the outcome. However, for other monoterpene-dominated environments, such as β-pinene and limonene, their unique ring structures[67] confer them a better tendency to undergo auto-oxidation forming more oxygenated RO_2, which may further form more oxygenated CHON dimers (thus less volatile) than α-pinene.[68] Therefore, the role of NO_3 chemistry in the biogenic NPF from these monoterpenes[69] is a worthy future effort to be explored in depth in controlled laboratory experiments. Our results highlight a need for a more realistic consideration of NPF processes in the atmosphere, especially when multiple oxidants/processes are involved. In addition, the influence of NO_3 derived from NO_x represents an anthropogenic perturbation on a biogenic system, which has broader implications for the understanding of aerosol sources and CCN in the modern atmosphere.

ASSOCIATED CONTENT

Supporting Information

The Supporting Information is available free of charge at https://pubs.acs.org/doi/10.1021/acs.est.3c07958.

Figures S1–S7, S10, S16, and S17 detail the lamps used; sensitivity comparison between mass spectrometers; effect of NO_3 radicals and NO on OVOC; evolution of normalized α-pinene reaction rate; simulation of the fate of $C_{10}H_{15}O_4$ and NO_3; Kendrick mass defect plots of OVOCs; and the volatility of CHO in the particle phase measured by FIGAERO-CIMS vs estimated by the VBS parametrizations for the CLOUD chamber experiments. Figures S8, S9, and S11–S15 present the gas phase precursors; Kendrick mass defect plots of OVOCs; simulated and observed low oxygenated OVOCs measured by CI-(NH_4^+)-Orbitrap; distribution of peroxy radicals; and sensitivity of NO_3 radicals to the formation of OVOCs for oxidation flow reactor experiments. Figures S18–S21 present nocturnal NPF event and nonevent measured by AIS; Kendrick mass defect plots of oxygenated compounds observed; time evolution of particle number, VOC, O_3, and estimated NO_3 in a nocturnal NPF event and nonevent; and monoterpene reaction rate in a nocturnal NPF event and nonevent during the Siikaneva campaign. (PDF)

AUTHOR INFORMATION

Corresponding Authors

Imad El-Haddad – *Laboratory of Atmospheric Chemistry, Paul Scherrer Institute, Villigen 5232, Switzerland;* orcid.org/0000-0002-2461-7238; Email: imad.el-haddad@psi.ch

Federico Bianchi – *Institute for Atmospheric and Earth System Research/Physics, Faculty of Science, University of Helsinki, Helsinki 00014, Finland;* orcid.org/0000-0003-2996-3604; Email: federico.bianchi@helsinki.fi

https://doi.org/10.1021/acs.est.3c07958
Environ. Sci. Technol. 2024, 58, 1601–1614

Matthieu Riva − *Univ Lyon, Université Claude Bernard Lyon 1, CNRS, IRCELYON, Villeurbanne 69626, France;* orcid.org/0000-0003-0054-4131; Email: matthieu.riva@ircelyon.univ-lyon1.fr

Authors

Dandan Li − *Univ Lyon, Université Claude Bernard Lyon 1, CNRS, IRCELYON, Villeurbanne 69626, France*

Wei Huang − *Institute for Atmospheric and Earth System Research/Physics, Faculty of Science, University of Helsinki, Helsinki 00014, Finland;* orcid.org/0000-0002-5049-2117

Dongyu Wang − *Laboratory of Atmospheric Chemistry, Paul Scherrer Institute, Villigen 5232, Switzerland*

Mingyi Wang − *Center for Atmospheric Particle Studies, Carnegie Mellon University, Pittsburgh, Pennsylvania 15213, United States;* Present Address: Now at the Division of Chemistry and Chemical Engineering, California Institute of Technology, Pasadena, California 91125, United States

Joel A. Thornton − *Department of Atmospheric Sciences, University of Washington, Seattle, Washington 98195, United States*

Lucía Caudillo − *Institute for Atmospheric and Environmental Sciences, Goethe University Frankfurt, Frankfurt am Main 60438, Germany*

Birte Rörup − *Institute for Atmospheric and Earth System Research/Physics, Faculty of Science, University of Helsinki, Helsinki 00014, Finland*

Ruby Marten − *Laboratory of Atmospheric Chemistry, Paul Scherrer Institute, Villigen 5232, Switzerland*

Wiebke Scholz − *Institute for Ion Physics and Applied Physics, University of Innsbruck, Innsbruck 6020, Austria*

Henning Finkenzeller − *Department of Chemistry & CIRES, University of Colorado Boulder, Boulder, Colorado 80309, United States*

Guillaume Marie − *Institute for Atmospheric and Environmental Sciences, Goethe University Frankfurt, Frankfurt am Main 60438, Germany*

Urs Baltensperger − *Laboratory of Atmospheric Chemistry, Paul Scherrer Institute, Villigen 5232, Switzerland*

David M. Bell − *Laboratory of Atmospheric Chemistry, Paul Scherrer Institute, Villigen 5232, Switzerland;* orcid.org/0000-0002-3958-2138

Zoé Brasseur − *Institute for Atmospheric and Earth System Research/Physics, Faculty of Science, University of Helsinki, Helsinki 00014, Finland;* orcid.org/0000-0001-5387-018X

Joachim Curtius − *Institute for Atmospheric and Environmental Sciences, Goethe University Frankfurt, Frankfurt am Main 60438, Germany*

Lubna Dada − *Laboratory of Atmospheric Chemistry, Paul Scherrer Institute, Villigen 5232, Switzerland*

Jonathan Duplissy − *Institute for Atmospheric and Earth System Research/Physics, Faculty of Science and Helsinki Institute of Physics (HIP)/Physics, Faculty of Science, University of Helsinki, Helsinki 00014, Finland;* orcid.org/0000-0001-8819-0264

Xianda Gong − *Leibniz Institute for Tropospheric Research, Leipzig 04318, Germany;* orcid.org/0000-0001-7274-0639

Armin Hansel − *Institute for Ion Physics and Applied Physics, University of Innsbruck, Innsbruck 6020, Austria;* orcid.org/0000-0002-1062-2394

Xu-Cheng He − *Institute for Atmospheric and Earth System Research/Physics, Faculty of Science, University of Helsinki, Helsinki 00014, Finland;* orcid.org/0000-0002-7416-306X

Victoria Hofbauer − *Center for Atmospheric Particle Studies, Carnegie Mellon University, Pittsburgh, Pennsylvania 15213, United States*

Heikki Junninen − *Institute of Physics, University of Tartu, Tartu 50090, Estonia*

Jordan E. Krechmer − *Aerodyne Research Inc., Billerica, Massachusetts 01821, United States*

Andreas Kürten − *Institute for Atmospheric and Environmental Sciences, Goethe University Frankfurt, Frankfurt am Main 60438, Germany*

Houssni Lamkaddam − *Laboratory of Atmospheric Chemistry, Paul Scherrer Institute, Villigen 5232, Switzerland*

Katrianne Lehtipalo − *Institute for Atmospheric and Earth System Research/Physics, Faculty of Science, University of Helsinki, Helsinki 00014, Finland; Finnish Meteorological Institute, Helsinki 00560, Finland*

Brandon Lopez − *Center for Atmospheric Particle Studies, Carnegie Mellon University, Pittsburgh, Pennsylvania 15213, United States*

Yingge Ma − *State Environmental Protection Key Laboratory of Formation and Prevention of Urban Air Pollution Complex, Shanghai Academy of Environment Sciences, Shanghai 200233, P. R. China*

Naser G. A. Mahfouz − *Atmospheric and Oceanic Sciences, Princeton University, Princeton, New Jersey 08540, United States*

Hanna E. Manninen − *CERN, the European Organization for Nuclear Research, Geneve 23 CH-1211, Switzerland*

Bernhard Mentler − *Institute for Ion Physics and Applied Physics, University of Innsbruck, Innsbruck 6020, Austria*

Sebastien Perrier − *Univ Lyon, Université Claude Bernard Lyon 1, CNRS, IRCELYON, Villeurbanne 69626, France*

Tuukka Petäjä − *Institute for Atmospheric and Earth System Research/Physics, Faculty of Science, University of Helsinki, Helsinki 00014, Finland*

Joschka Pfeifer − *CERN, the European Organization for Nuclear Research, Geneve 23 CH-1211, Switzerland*

Maxim Philippov − *P.N. Lebedev Physical Institute of the Russian Academy of Sciences, Moscow 119991, Russia;* orcid.org/0000-0003-4302-0020

Meredith Schervish − *Center for Atmospheric Particle Studies, Carnegie Mellon University, Pittsburgh, Pennsylvania 15213, United States*

Siegfried Schobesberger − *Department of Applied Physics, University of Eastern Finland, Kuopio 70211, Finland*

Jiali Shen − *Institute for Atmospheric and Earth System Research/Physics, Faculty of Science, University of Helsinki, Helsinki 00014, Finland;* orcid.org/0000-0001-8701-7929

Mihnea Surdu − *Laboratory of Atmospheric Chemistry, Paul Scherrer Institute, Villigen 5232, Switzerland;* orcid.org/0000-0003-1815-2750

Sophie Tomaz − *Univ Lyon, Université Claude Bernard Lyon 1, CNRS, IRCELYON, Villeurbanne 69626, France*

Rainer Volkamer − *Department of Chemistry & CIRES, University of Colorado Boulder, Boulder, Colorado 80309, United States;* orcid.org/0000-0002-0899-1369

Xinke Wang − *Univ Lyon, Université Claude Bernard Lyon 1, CNRS, IRCELYON, Villeurbanne 69626, France*

https://doi.org/10.1021/acs.est.3c07958
Environ. Sci. Technol. 2024, 58, 1601−1614

Stefan K. Weber − *Institute for Atmospheric and Environmental Sciences, Goethe University Frankfurt, Frankfurt am Main 60438, Germany; CERN, the European Organization for Nuclear Research, Geneve 23 CH-1211, Switzerland*
André Welti − *Finnish Meteorological Institute, Helsinki 00560, Finland*
Douglas R. Worsnop − *Institute for Atmospheric and Earth System Research/Physics, Faculty of Science, University of Helsinki, Helsinki 00014, Finland; Aerodyne Research Inc., Billerica, Massachusetts 01821, United States*
Yusheng Wu − *Institute for Atmospheric and Earth System Research/Physics, Faculty of Science, University of Helsinki, Helsinki 00014, Finland*
Chao Yan − *Institute for Atmospheric and Earth System Research/Physics, Faculty of Science, University of Helsinki, Helsinki 00014, Finland*
Marcel Zauner-Wieczorek − *Institute for Atmospheric and Environmental Sciences, Goethe University Frankfurt, Frankfurt am Main 60438, Germany*
Markku Kulmala − *Institute for Atmospheric and Earth System Research/Physics, Faculty of Science, University of Helsinki, Helsinki 00014, Finland*
Jasper Kirkby − *Institute for Atmospheric and Environmental Sciences, Goethe University Frankfurt, Frankfurt am Main 60438, Germany; CERN, the European Organization for Nuclear Research, Geneve 23 CH-1211, Switzerland*
Neil M. Donahue − *Center for Atmospheric Particle Studies, Carnegie Mellon University, Pittsburgh, Pennsylvania 15213, United States;* orcid.org/0000-0003-3054-2364
Christian George − *Univ Lyon, Université Claude Bernard Lyon 1, CNRS, IRCELYON, Villeurbanne 69626, France;* orcid.org/0000-0003-1578-7056

Complete contact information is available at: https://pubs.acs.org/10.1021/acs.est.3c07958

Author Contributions

[✓]D.L. and W.H contributed equally. The manuscript was written through contributions of all authors. D.D.L., D.Y.W., M.Y.W., L.C., B.R., R.M., W.S., H.F., G.M., D.M.B., Z.B., J.C., L.D., J.D., X.D.G., A.H., X.-C.H., V.H., H.J., J.E.K., A.K., H.L., K.L., B.L., N.G.A.M., H.E.M., B.M., S.P., J.P., M.P., M.S., S.S., J.L.S., M.S., S.T., R.V., X.K.W., S.K.W., A.W., D.R.W., Y.S.W., M.Z.-W., M.K., J.K., N.M.D., C.G., I.E.-H., and M.R. prepared the CLOUD facility or measuring instruments. D.D.L., D.Y.W., M.Y.W., L.C., B.R., R.M., W.S., H.F., G.M., D.M.B., J.D., X.D.G., X.-C.H., V.H., H.L., B.L., N.G.A.M., B.M., M.S., J.L.S., M.S., S.K.W., Y.S.W., M.Z.-W., J.K., and M.R. collected the CLOUD data. D.D.L., W.H., D.Y.W., M.Y.W., L.C., B.R., R.M., W.S., H.F., G.M., H.L., S.K.W., and M.R. analyzed the data. D.D.L., D.Y.W., S.P., C.G., I.E.-H., and M.R. planned the flow tube experiments. W.H., H.J., T.P., M.K., and F.B. planned the field campaign and/or data analysis. D.D.L., J.A.T., and M.R. provided model calculations. D.D.L., W.H., D.Y.W., M.Y.W., J.A.T., L.C., B.R., R.M., W.S., H.F., U.B., X.D.G., A.H., H.J., K.L., Y.G.M., B.M., S.P., T.P., S.T., R.V., X.K.W., C.Y., J.K., N.M.D., C.G., I.E.-H., F.B., and M.R. contributed to the scientific discussion. D.D.L., W.H., D.Y.W., M.Y.W., J.A.T., U.B., N.M.D., C.G., I.E.-H., F.B., and M.R. wrote the manuscript. All authors discussed the results and commented on the paper. All authors have given approval to the final version of the manuscript.

Funding

This work was financially supported by the French National program LEFE (Les Enveloppes Fluides et l'Environnement), the European Research Council (ERC-StG MAARvEL; no. 852161 and ERC-StG CHAPAs; no. 850614), the European Union's Horizon 2020 Research and Innovation program (Marie Sklodowska-Curie Grant Agreement no. 764991), the Swiss National Science Foundation (200020_172602 and 20FI20_172622), and the US National Science Foundation (AGS-1801574, AGS-1801897, AGS-2132089, and AGS-1801280). The PSI team thanks the European Commission Horizon 2020 Research and Innovation Framework Program, ATMO-ACCESS Integrating Activity (grant agreement no. 101008004). D.D.L. thanks the China Scholarship Council of P. R. China for the Ph.D. grant and support by the State Environment Protection Key Laboratory of Formation and Prevention of Urban Air Pollution Complex (CX2020080582). J.A.T. was supported with a grant from the U.S. Department of Energy Atmospheric System Research Program (DE-SC0021097). H.J. thanks the European Regional Development Fund (project MOBTT42) and Estonian Research Council (project PRG714).

Notes

The authors declare no competing financial interest.

■ ACKNOWLEDGMENTS

We thank the European Organization for Nuclear Research (CERN) for supporting CLOUD with important technical and financial resources. We thank the Orbitool team for developing the tools to analyze mass spectra and the F0AM people for developing systems to simulate atmospheric chemistry. W.S. thanks the University of Innsbruck for her doctoral scholarship (2021/1). X.C.H. thanks Jenny and Antti Wihuri Foundation for providing funding for this research.

■ REFERENCES

(1) Kulmala, M.; Vehkamäki, H.; Petäjä, T.; Dal Maso, M.; Lauri, A.; Kerminen, V.-M.; Birmili, W.; McMurry, P. Formation and growth rates of ultrafine atmospheric particles: a review of observations. *J. Aerosol Sci.* **2004**, *35* (2), 143−176.
(2) Kerminen, V. M.; Petäjä, T.; Manninen, H. E.; Paasonen, P.; Nieminen, T.; Sipilä, M.; Junninen, H.; Ehn, M.; Gagné, S.; Laakso, L.; Riipinen, I.; Vehkamäki, H.; Kurten, T.; Ortega, I. K.; Dal Maso, M.; Brus, D.; Hyvärinen, A.; Lihavainen, H.; Leppä, J.; Lehtinen, K. E. J.; Mirme, A.; Mirme, S.; Hõrrak, U.; Berndt, T.; Stratmann, F.; Birmili, W.; Wiedensohler, A.; Metzger, A.; Dommen, J.; Baltensperger, U.; Kiendler-Scharr, A.; Mentel, T. F.; Wildt, J.; Winkler, P. M.; Wagner, P. E.; Petzold, A.; Minikin, A.; Plass-Dülmer, C.; Pöschl, U.; Laaksonen, A.; Kulmala, M. Atmospheric nucleation: highlights of the EUCAARI project and future directions. *Atmospheric Chemistry and Physics* **2010**, *10* (22), 10829−10848.
(3) Bianchi, F.; Kurten, T.; Riva, M.; Mohr, C.; Rissanen, M. P.; Roldin, P.; Berndt, T.; Crounse, J. D.; Wennberg, P. O.; Mentel, T. F.; Wildt, J.; Junninen, H.; Jokinen, T.; Kulmala, M.; Worsnop, D. R.; Thornton, J. A.; Donahue, N.; Kjaergaard, H. G.; Ehn, M. Highly Oxygenated Organic Molecules (HOM) from Gas-Phase Autoxidation Involving Peroxy Radicals: A Key Contributor to Atmospheric Aerosol. *Chem. Rev.* **2019**, *119* (6), 3472−3509.
(4) Trostl, J.; Chuang, W. K.; Gordon, H.; Heinritzi, M.; Yan, C.; Molteni, U.; Ahlm, L.; Frege, C.; Bianchi, F.; Wagner, R.; Simon, M.; Lehtipalo, K.; Williamson, C.; Craven, J. S.; Duplissy, J.; Adamov, A.; Almeida, J.; Bernhammer, A. K.; Breitenlechner, M.; Brilke, S.; Dias, A.; Ehrhart, S.; Flagan, R. C.; Franchin, A.; Fuchs, C.; Guida, R.; Gysel, M.; Hansel, A.; Hoyle, C. R.; Jokinen, T.; Junninen, H.; Kangasluoma, J.; Keskinen, H.; Kim, J.; Krapf, M.; Kurten, A.;

Laaksonen, A.; Lawler, M.; Leiminger, M.; Mathot, S.; Mohler, O.; Nieminen, T.; Onnela, A.; Petaja, T.; Piel, F. M.; Miettinen, P.; Rissanen, M. P.; Rondo, L.; Sarnela, N.; Schobesberger, S.; Sengupta, K.; Sipila, M.; Smith, J. N.; Steiner, G.; Tome, A.; Virtanen, A.; Wagner, A. C.; Weingartner, E.; Wimmer, D.; Winkler, P. M.; Ye, P.; Carslaw, K. S.; Curtius, J.; Dommen, J.; Kirkby, J.; Kulmala, M.; Riipinen, I.; Worsnop, D. R.; Donahue, N. M.; Baltensperger, U. The role of low-volatility organic compounds in initial particle growth in the atmosphere. *Nature* **2016**, *533* (7604), 527−31.

(5) Ehn, M.; Thornton, J. A.; Kleist, E.; Sipila, M.; Junninen, H.; Pullinen, I.; Springer, M.; Rubach, F.; Tillmann, R.; Lee, B.; Lopez-Hilfiker, F.; Andres, S.; Acir, I. H.; Rissanen, M.; Jokinen, T.; Schobesberger, S.; Kangasluoma, J.; Kontkanen, J.; Nieminen, T.; Kurten, T.; Nielsen, L. B.; Jorgensen, S.; Kjaergaard, H. G.; Canagaratna, M.; Maso, M. D.; Berndt, T.; Petaja, T.; Wahner, A.; Kerminen, V. M.; Kulmala, M.; Worsnop, D. R.; Wildt, J.; Mentel, T. F. A large source of low-volatility secondary organic aerosol. *Nature* **2014**, *506* (7489), 476−9.

(6) Kirkby, J.; Duplissy, J.; Sengupta, K.; Frege, C.; Gordon, H.; Williamson, C.; Heinritzi, M.; Simon, M.; Yan, C.; Almeida, J.; Tröstl, J.; Nieminen, T.; Ortega, I. K.; Wagner, R.; Adamov, A.; Amorim, A.; Bernhammer, A.-K.; Bianchi, F.; Breitenlechner, M.; Brilke, S.; Chen, X.; Craven, J.; Dias, A.; Ehrhart, S.; Flagan, R. C.; Franchin, A.; Fuchs, C.; Guida, R.; Hakala, J.; Hoyle, C. R.; Jokinen, T.; Junninen, H.; Kangasluoma, J.; Kim, J.; Krapf, M.; Kürten, A.; Laaksonen, A.; Lehtipalo, K.; Makhmutov, V.; Mathot, S.; Molteni, U.; Onnela, A.; Peräkylä, O.; Piel, F.; Petäjä, T.; Praplan, A. P.; Pringle, K.; Rap, A.; Richards, N. A. D.; Riipinen, I.; Rissanen, M. P.; Rondo, L.; Sarnela, N.; Schobesberger, S.; Scott, C. E.; Seinfeld, J. H.; Sipilä, M.; Steiner, G.; Stozhkov, Y.; Stratmann, F.; Tomé, A.; Virtanen, A.; Vogel, A. L.; Wagner, A. C.; Wagner, P. E.; Weingartner, E.; Wimmer, D.; Winkler, P. M.; Ye, P.; Zhang, X.; Hansel, A.; Dommen, J.; Donahue, N. M.; Worsnop, D. R.; Baltensperger, U.; Kulmala, M.; Carslaw, K. S.; Curtius, J. Ion-induced nucleation of pure biogenic particles. *Nature* **2016**, *533*, 521.

(7) Bianchi, F.; Tröstl, J.; Junninen, H.; Frege, C.; Henne, S.; Hoyle, C. R.; Molteni, U.; Herrmann, E.; Adamov, A.; Bukowiecki, N.; Chen, X.; Duplissy, J.; Gysel, M.; Hutterli, M.; Kangasluoma, J.; Kontkanen, J.; Kürten, A.; Manninen, H. E.; Münch, S.; Peräkylä, O.; Petäjä, T.; Rondo, L.; Williamson, C.; Weingartner, E.; Curtius, J.; Worsnop, D. R.; Kulmala, M.; Dommen, J.; Baltensperger, U. New particle formation in the free troposphere: A question of chemistry and timing. *Science* **2016**, *352* (6289), 1109−1112.

(8) Kürten, A.; Bergen, A.; Heinritzi, M.; Leiminger, M.; Lorenz, V.; Piel, F.; Simon, M.; Sitals, R.; Wagner, A. C.; Curtius, J. Observation of new particle formation and measurement of sulfuric acid, ammonia, amines and highly oxidized organic molecules at a rural site in central Germany. *Atmospheric Chemistry and Physics* **2016**, *16* (19), 12793−12813.

(9) Rose, C.; Zha, Q.; Dada, L.; Yan, C.; Lehtipalo, K.; Junninen, H.; Mazon, S. B.; Jokinen, T.; Sarnela, N.; Sipilä, M.; Petäjä, T.; Kerminen, V.-M.; Bianchi, F.; Kulmala, M. Observations of biogenic ion-induced cluster formation in the atmosphere. *Sci. Adv.* **2018**, *4* (4), No. eaar5218.

(10) Almeida, J.; Schobesberger, S.; Kurten, A.; Ortega, I. K.; Kupiainen-Maatta, O.; Praplan, A. P.; Adamov, A.; Amorim, A.; Bianchi, F.; Breitenlechner, M.; David, A.; Dommen, J.; Donahue, N. M.; Downard, A.; Dunne, E.; Duplissy, J.; Ehrhart, S.; Flagan, R. C.; Franchin, A.; Guida, R.; Hakala, J.; Hansel, A.; Heinritzi, M.; Henschel, H.; Jokinen, T.; Junninen, H.; Kajos, M.; Kangasluoma, J.; Keskinen, H.; Kupc, A.; Kurten, T.; Kvashin, A. N.; Laaksonen, A.; Lehtipalo, K.; Leiminger, M.; Leppa, J.; Loukonen, V.; Makhmutov, V.; Mathot, S.; McGrath, M. J.; Nieminen, T.; Olenius, T.; Onnela, A.; Petaja, T.; Riccobono, F.; Riipinen, I.; Rissanen, M.; Rondo, L.; Ruuskanen, T.; Santos, F. D.; Sarnela, N.; Schallhart, S.; Schnitzhofer, R.; Seinfeld, J. H.; Simon, M.; Sipila, M.; Stozhkov, Y.; Stratmann, F.; Tome, A.; Trostl, J.; Tsagkogeorgas, G.; Vaattovaara, P.; Viisanen, Y.; Virtanen, A.; Vrtala, A.; Wagner, P. E.; Weingartner, E.; Wex, H.; Williamson, C.; Wimmer, D.; Ye, P.; Yli-Juuti, T.; Carslaw, K. S.; Kulmala, M.; Curtius, J.; Baltensperger, U.; Worsnop, D. R.; Vehkamaki, H.; Kirkby, J. Molecular understanding of sulphuric acid-amine particle nucleation in the atmosphere. *Nature* **2013**, *502* (7471), 359−63.

(11) Wang, M.; Kong, W.; Marten, R.; He, X.-C.; Chen, D.; Pfeifer, J.; Heitto, A.; Kontkanen, J.; Dada, L.; Kürten, A.; Yli-Juuti, T.; Manninen, H. E.; Amanatidis, S.; Amorim, A.; Baalbaki, R.; Baccarini, A.; Bell, D. M.; Bertozzi, B.; Bräkling, S.; Brilke, S.; Murillo, L. C.; Chiu, R.; Chu, B.; De Menezes, L.-P.; Duplissy, J.; Finkenzeller, H.; Carracedo, L. G.; Granzin, M.; Guida, R.; Hansel, A.; Hofbauer, V.; Krechmer, J.; Lehtipalo, K.; Lamkaddam, H.; Lampimäki, M.; Lee, C. P.; Makhmutov, V.; Marie, G.; Mathot, S.; Mauldin, R. L.; Mentler, B.; Müller, T.; Onnela, A.; Partoll, E.; Petäjä, T.; Philippov, M.; Pospisilova, V.; Ranjithkumar, A.; Rissanen, M.; Rörup, B.; Scholz, W.; Shen, J.; Simon, M.; Sipilä, M.; Steiner, G.; Stolzenburg, D.; Tham, Y. J.; Tomé, A.; Wagner, A. C.; Wang, D. S.; Wang, Y.; Weber, S. K.; Winkler, P. M.; Wlasits, P. J.; Wu, Y.; Xiao, M.; Ye, Q.; Zauner-Wieczorek, M.; Zhou, X.; Volkamer, R.; Riipinen, I.; Dommen, J.; Curtius, J.; Baltensperger, U.; Kulmala, M.; Worsnop, D. R.; Kirkby, J.; Seinfeld, J. H.; El-Haddad, I.; Flagan, R. C.; Donahue, N. M. Rapid growth of new atmospheric particles by nitric acid and ammonia condensation. *Nature* **2020**, *581* (7807), 184−189.

(12) He, X. C.; Tham, Y. J.; Dada, L.; Wang, M.; Finkenzeller, H.; Stolzenburg, D.; Iyer, S.; Simon, M.; Kurten, A.; Shen, J.; Rorup, B.; Rissanen, M.; Schobesberger, S.; Baalbaki, R.; Wang, D. S.; Koenig, T. K.; Jokinen, T.; Sarnela, N.; Beck, L. J.; Almeida, J.; Amanatidis, S.; Amorim, A.; Ataei, F.; Baccarini, A.; Bertozzi, B.; Bianchi, F.; Brilke, S.; Caudillo, L.; Chen, D.; Chiu, R.; Chu, B.; Dias, A.; Ding, A.; Dommen, J.; Duplissy, J.; El Haddad, I.; Gonzalez Carracedo, L.; Granzin, M.; Hansel, A.; Heinritzi, M.; Hofbauer, V.; Junninen, H.; Kangasluoma, J.; Kemppainen, D.; Kim, C.; Kong, W.; Krechmer, J. E.; Kvashin, A.; Laitinen, T.; Lamkaddam, H.; Lee, C. P.; Lehtipalo, K.; Leiminger, M.; Li, Z.; Makhmutov, V.; Manninen, H. E.; Marie, G.; Marten, R.; Mathot, S.; Mauldin, R. L.; Mentler, B.; Mohler, O.; Muller, T.; Nie, W.; Onnela, A.; Petaja, T.; Pfeifer, J.; Philippov, M.; Ranjithkumar, A.; Saiz-Lopez, A.; Salma, I.; Scholz, W.; Schuchmann, S.; Schulze, B.; Steiner, G.; Stozhkov, Y.; Tauber, C.; Tome, A.; Thakur, R. C.; Vaisanen, O.; Vazquez-Pufleau, M.; Wagner, A. C.; Wang, Y.; Weber, S. K.; Winkler, P. M.; Wu, Y.; Xiao, M.; Yan, C.; Ye, Q.; Ylisirnio, A.; Zauner-Wieczorek, M.; Zha, Q.; Zhou, P.; Flagan, R. C.; Curtius, J.; Baltensperger, U.; Kulmala, M.; Kerminen, V. M.; Kurten, T.; Donahue, N. M.; Volkamer, R.; Kirkby, J.; Worsnop, D. R.; Sipila, M. Role of iodine oxoacids in atmospheric aerosol nucleation. *Science* **2021**, *371* (6529), 589−595.

(13) Wang, M.; Xiao, M.; Bertozzi, B.; Marie, G.; Rorup, B.; Schulze, B.; Bardakov, R.; He, X. C.; Shen, J.; Scholz, W.; Marten, R.; Dada, L.; Baalbaki, R.; Lopez, B.; Lamkaddam, H.; Manninen, H. E.; Amorim, A.; Ataei, F.; Bogert, P.; Brasseur, Z.; Caudillo, L.; De Menezes, L. P.; Duplissy, J.; Ekman, A. M. L.; Finkenzeller, H.; Carracedo, L. G.; Granzin, M.; Guida, R.; Heinritzi, M.; Hofbauer, V.; Hohler, K.; Korhonen, K.; Krechmer, J. E.; Kurten, A.; Lehtipalo, K.; Mahfouz, N. G. A.; Makhmutov, V.; Massabo, D.; Mathot, S.; Mauldin, R. L.; Mentler, B.; Muller, T.; Onnela, A.; Petaja, T.; Philippov, M.; Piedehierro, A. A.; Pozzer, A.; Ranjithkumar, A.; Schervish, M.; Schobesberger, S.; Simon, M.; Stozhkov, Y.; Tome, A.; Umo, N. S.; Vogel, F.; Wagner, R.; Wang, D. S.; Weber, S. K.; Welti, A.; Wu, Y.; Zauner-Wieczorek, M.; Sipila, M.; Winkler, P. M.; Hansel, A.; Baltensperger, U.; Kulmala, M.; Flagan, R. C.; Curtius, J.; Riipinen, I.; Gordon, H.; Lelieveld, J.; El-Haddad, I.; Volkamer, R.; Worsnop, D. R.; Christoudias, T.; Kirkby, J.; Mohler, O.; Donahue, N. M. Synergistic HNO_3-H_2SO_4-NH_3 upper tropospheric particle formation. *Nature* **2022**, *605* (7910), 483−489.

(14) Jimenez, J. L.; Canagaratna, M. R.; Donahue, N. M.; Prevot, A. S. H.; Zhang, Q.; Kroll, J. H.; DeCarlo, P. F.; Allan, J. D.; Coe, H.; Ng, N. L.; Aiken, A. C.; Docherty, K. S.; Ulbrich, I. M.; Grieshop, A. P.; Robinson, A. L.; Duplissy, J.; Smith, J. D.; Wilson, K. R.; Lanz, V. A.; Hueglin, C.; Sun, Y. L.; Tian, J.; Laaksonen, A.; Raatikainen, T.; Rautiainen, J.; Vaattovaara, P.; Ehn, M.; Kulmala, M.; Tomlinson, J. M.; Collins, D. R.; Cubison, M. J.; Dunlea, J.; Huffman, J. A.; Onasch,

https://doi.org/10.1021/acs.est.3c07958
Environ. Sci. Technol. 2024, 58, 1601−1614

T. B.; Alfarra, M. R.; Williams, P. I.; Bower, K.; Kondo, Y.; Schneider, J.; Drewnick, F.; Borrmann, S.; Weimer, S.; Demerjian, K.; Salcedo, D.; Cottrell, L.; Griffin, R.; Takami, A.; Miyoshi, T.; Hatakeyama, S.; Shimono, A.; Sun, J. Y.; Zhang, Y. M.; Dzepina, K.; Kimmel, J. R.; Sueper, D.; Jayne, J. T.; Herndon, S. C.; Trimborn, A. M.; Williams, L. R.; Wood, E. C.; Middlebrook, A. M.; Kolb, C. E.; Baltensperger, U.; Worsnop, D. R. Evolution of Organic Aerosols in the Atmosphere. *Science* **2009**, *326* (5959), 1525−1529.

(15) Gordon, H.; Sengupta, K.; Rap, A.; Duplissy, J.; Frege, C.; Williamson, C.; Heinritzi, M.; Simon, M.; Yan, C.; Almeida, J.; Trostl, J.; Nieminen, T.; Ortega, I. K.; Wagner, R.; Dunne, E. M.; Adamov, A.; Amorim, A.; Bernhammer, A. K.; Bianchi, F.; Breitenlechner, M.; Brilke, S.; Chen, X.; Craven, J. S.; Dias, A.; Ehrhart, S.; Fischer, L.; Flagan, R. C.; Franchin, A.; Fuchs, C.; Guida, R.; Hakala, J.; Hoyle, C. R.; Jokinen, T.; Junninen, H.; Kangasluoma, J.; Kim, J.; Kirkby, J.; Krapf, M.; Kurten, A.; Laaksonen, A.; Lehtipalo, K.; Makhmutov, V.; Mathot, S.; Molteni, U.; Monks, S. A.; Onnela, A.; Perakyla, O.; Piel, F.; Petaja, T.; Praplan, A. P.; Pringle, K. J.; Richards, N. A.; Rissanen, M. P.; Rondo, L.; Sarnela, N.; Schobesberger, S.; Scott, C. E.; Seinfeld, J. H.; Sharma, S.; Sipila, M.; Steiner, G.; Stozhkov, Y.; Stratmann, F.; Tome, A.; Virtanen, A.; Vogel, A. L.; Wagner, A. C.; Wagner, P. E.; Weingartner, E.; Wimmer, D.; Winkler, P. M.; Ye, P.; Zhang, X.; Hansel, A.; Dommen, J.; Donahue, N. M.; Worsnop, D. R.; Baltensperger, U.; Kulmala, M.; Curtius, J.; Carslaw, K. S. Reduced anthropogenic aerosol radiative forcing caused by biogenic new particle formation. *Proc. Natl. Acad. Sci. U. S. A.* **2016**, *113* (43), 12053−12058.

(16) Gordon, H.; Kirkby, J.; Baltensperger, U.; Bianchi, F.; Breitenlechner, M.; Curtius, J.; Dias, A.; Dommen, J.; Donahue, N. M.; Dunne, E. M.; Duplissy, J.; Ehrhart, S.; Flagan, R. C.; Frege, C.; Fuchs, C.; Hansel, A.; Hoyle, C. R.; Kulmala, M.; Kürten, A.; Lehtipalo, K.; Makhmutov, V.; Molteni, U.; Rissanen, M. P.; Stozkhov, Y.; Tröstl, J.; Tsagkogeorgas, G.; Wagner, R.; Williamson, C.; Wimmer, D.; Winkler, P. M.; Yan, C.; Carslaw, K. S. Causes and importance of new particle formation in the present-day and preindustrial atmospheres. *Journal of Geophysical Research: Atmospheres* **2017**, *122* (16), 8739−8760.

(17) Molteni, U.; Bianchi, F.; Klein, F.; El Haddad, I.; Frege, C.; Rossi, M. J.; Dommen, J.; Baltensperger, U. Formation of highly oxygenated organic molecules from aromatic compounds. *Atmospheric Chemistry and Physics* **2018**, *18* (3), 1909−1921.

(18) Berndt, T.; Scholz, W.; Mentler, B.; Fischer, L.; Herrmann, H.; Kulmala, M.; Hansel, A. Accretion Product Formation from Self- and Cross-Reactions of RO_2 Radicals in the Atmosphere. *Angew. Chem.* **2018**, *57* (14), 3820−3824.

(19) Zhao, Y.; Thornton, J. A.; Pye, H. O. T. Quantitative constraints on autoxidation and dimer formation from direct probing of monoterpene-derived peroxy radical chemistry. *Proc. Natl. Acad. Sci. U. S. A.* **2018**, *115* (48), 12142−12147.

(20) Tomaz, S.; Wang, D.; Zabalegui, N.; Li, D.; Lamkaddam, H.; Bachmeier, F.; Vogel, A.; Monge, M. E.; Perrier, S.; Baltensperger, U.; George, C.; Rissanen, M.; Ehn, M.; El Haddad, I.; Riva, M. Structures and reactivity of peroxy radicals and dimeric products revealed by online tandem mass spectrometry. *Nat. Commun.* **2021**, *12* (1), 300.

(21) Jokinen, T.; Berndt, T.; Makkonen, R.; Kerminen, V. M.; Junninen, H.; Paasonen, P.; Stratmann, F.; Herrmann, H.; Guenther, A. B.; Worsnop, D. R.; Kulmala, M.; Ehn, M.; Sipila, M. Production of extremely low volatile organic compounds from biogenic emissions: Measured yields and atmospheric implications. *Proc. Natl. Acad. Sci. U. S. A.* **2015**, *112* (23), 7123−8.

(22) Lim, Y. B.; Ziemann, P. J. Products and Mechanism of Secondary Organic Aerosol Formation from Reactions of n-Alkanes with OH Radicals in the Presence of NO_x. *Environ. Sci. Technol.* **2005**, *39* (23), 9229−9236.

(23) Kurtenbach, R.; Ackermann, R.; Becker, K. H.; Geyer, A.; Gomes, J. A. G.; Lörzer, J. C.; Platt, U.; Wiesen, P. Verification of the Contribution of Vehicular Traffic to the Total NMVOC Emissions in Germany and the Importance of the NO_3 Chemistry in the City Air. *Journal of Atmospheric Chemistry* **2002**, *42* (1), 395−411.

(24) Asaf, D.; Pedersen, D.; Matveev, V.; Peleg, M.; Kern, C.; Zingler, J.; Platt, U.; Luria, M. Long-Term Measurements of NO3 Radical at a Semiarid Urban Site: 1. Extreme Concentration Events and Their Oxidation Capacity. *Environ. Sci. Technol.* **2009**, *43* (24), 9117−9123.

(25) Geyer, A.; Alicke, B.; Konrad, S.; Schmitz, T.; Stutz, J.; Platt, U. Chemistry and oxidation capacity of the nitrate radical in the continental boundary layer near Berlin. *Journal of Geophysical Research: Atmospheres* **2001**, *106* (D8), 8013−8025.

(26) Kulmala, M.; Hämeri, K.; Aalto, P. P.; Mäkelä, J. M.; Pirjola, L.; Nilsson, E. D.; Buzorius, G.; Rannik, Ü.; Dal Maso, M.; Seidl, W.; Hoffman, T.; Janson, R.; Hansson, H. C.; Viisanen, Y.; Laaksonen, A.; O'dowd, C. D. Overview of the international project on biogenic aerosol formation in the boreal forest (BIOFOR). *Tellus B* **2001**, *53* (4), 324−343.

(27) Junninen, H.; Hulkkonen, M.; Riipinen, I.; Nieminen, T.; Hirsikko, A.; Suni, T.; Boy, M.; Lee, S.-H.; Vana, M.; Tammet, H.; Kerminen, V.-M.; Kulmala, M. Observations on nocturnal growth of atmospheric clusters. *Tellus B* **2017**, *60* (3), 365−371.

(28) Bonn, B.; Moorgat, G. K. New particle formation during α- and β-pinene oxidation by O_3, OH and NO_3, and the influence of water vapour: particle size distribution studies. *Atmospheric Chemistry and Physics* **2002**, *2* (3), 183−196.

(29) Yan, C.; Nie, W.; Äijälä, M.; Rissanen, M. P.; Canagaratna, M. R.; Massoli, P.; Junninen, H.; Jokinen, T.; Sarnela, N.; Häme, S. A. K.; Schobesberger, S.; Canonaco, F.; Yao, L.; Prévôt, A. S. H.; Petäjä, T.; Kulmala, M.; Sipilä, M.; Worsnop, D. R.; Ehn, M. Source characterization of highly oxidized multifunctional compounds in a boreal forest environment using positive matrix factorization. *Atmospheric Chemistry and Physics* **2016**, *16* (19), 12715−12731.

(30) Fry, J. L.; Draper, D. C.; Barsanti, K. C.; Smith, J. N.; Ortega, J.; Winkler, P. M.; Lawler, M. J.; Brown, S. S.; Edwards, P. M.; Cohen, R. C.; Lee, L. Secondary organic aerosol formation and organic nitrate yield from NO3 oxidation of biogenic hydrocarbons. *Environ. Sci. Technol.* **2014**, *48* (20), 11944−53.

(31) Ng, N. L.; Brown, S. S.; Archibald, A. T.; Atlas, E.; Cohen, R. C.; Crowley, J. N.; Day, D. A.; Donahue, N. M.; Fry, J. L.; Fuchs, H.; Griffin, R. J.; Guzman, M. I.; Herrmann, H.; Hodzic, A.; Iinuma, Y.; Jimenez, J. L.; Kiendler-Scharr, A.; Lee, B. H.; Luecken, D. J.; Mao, J.; McLaren, R.; Mutzel, A.; Osthoff, H. D.; Ouyang, B.; Picquet-Varrault, B.; Platt, U.; Pye, H. O. T.; Rudich, Y.; Schwantes, R. H.; Shiraiwa, M.; Stutz, J.; Thornton, J. A.; Tilgner, A.; Williams, B. J.; Zaveri, R. A. Nitrate radicals and biogenic volatile organic compounds: oxidation, mechanisms, and organic aerosol. *Atmospheric Chemistry and Physics* **2017**, *17* (3), 2103−2162.

(32) Bates, K. H.; Burke, G. J. P.; Cope, J. D.; Nguyen, T. B. Secondary organic aerosol and organic nitrogen yields from the nitrate radical (NO_3) oxidation of alpha-pinene from various RO_2 fates. *Atmospheric Chemistry and Physics* **2022**, *22* (2), 1467−1482.

(33) Aregahegn, K. Z.; Nozière, B.; George, C. Organic aerosol formation photo-enhanced by the formation of secondary photosensitizers in aerosols. *Faraday Discuss.* **2013**, *165*, 123.

(34) Riva, M.; Ehn, M.; Li, D.; Tomaz, S.; Bourgain, F.; Perrier, S.; George, C. CI-Orbitrap: An Analytical Instrument To Study Atmospheric Reactive Organic Species. *Anal. Chem.* **2019**, *91* (15), 9419−9423.

(35) Kurten, A.; Jokinen, T.; Simon, M.; Sipila, M.; Sarnela, N.; Junninen, H.; Adamov, A.; Almeida, J.; Amorim, A.; Bianchi, F.; Breitenlechner, M.; Dommen, J.; Donahue, N. M.; Duplissy, J.; Ehrhart, S.; Flagan, R. C.; Franchin, A.; Hakala, J.; Hansel, A.; Heinritzi, M.; Hutterli, M.; Kangasluoma, J.; Kirkby, J.; Laaksonen, A.; Lehtipalo, K.; Leiminger, M.; Makhmutov, V.; Mathot, S.; Onnela, A.; Petaja, T.; Praplan, A. P.; Riccobono, F.; Rissanen, M. P.; Rondo, L.; Schobesberger, S.; Seinfeld, J. H.; Steiner, G.; Tome, A.; Trostl, J.; Winkler, P. M.; Williamson, C.; Wimmer, D.; Ye, P.; Baltensperger, U.; Carslaw, K. S.; Kulmala, M.; Worsnop, D. R.; Curtius, J. Neutral molecular cluster formation of sulfuric acid-dimethylamine observed in real time under atmospheric conditions. *Proc. Natl. Acad. Sci. U. S. A.* **2014**, *111* (42), 15019−24.

https://doi.org/10.1021/acs.est.3c07958
Environ. Sci. Technol. 2024, 58, 1601−1614

(36) Breitenlechner, M.; Fischer, L.; Hainer, M.; Heinritzi, M.; Curtius, J.; Hansel, A. PTR3: An Instrument for Studying the Lifecycle of Reactive Organic Carbon in the Atmosphere. *Anal. Chem.* **2017**, *89* (11), 5824−5831.
(37) Dada, L.; Lehtipalo, K.; Kontkanen, J.; Nieminen, T.; Baalbaki, R.; Ahonen, L.; Duplissy, J.; Yan, C.; Chu, B.; Petaja, T.; Lehtinen, K.; Kerminen, V. M.; Kulmala, M.; Kangasluoma, J. Formation and growth of sub-3-nm aerosol particles in experimental chambers. *Nat. Protoc.* **2020**, *15* (3), 1013−1040.
(38) Mai, H.; Flagan, R. C. Scanning DMA Data Analysis I. Classification Transfer Function. *Aerosol Sci. Technol.* **2018**, *52* (12), 1382−1399.
(39) Riva, M.; Brüggemann, M.; Li, D.; Perrier, S.; George, C.; Herrmann, H.; Berndt, T. Capability of CI-Orbitrap for Gas-Phase Analysis in Atmospheric Chemistry: A Comparison with the CI-APi-TOF Technique. *Anal. Chem.* **2020**, *92* (12), 8142−8150.
(40) Lindinger, W.; Hansel, A.; Jordan, A. On-line monitoring of volatile organic compounds at pptv levels by means of proton-transfer-reaction mass spectrometry (PTR-MS) medical applications, food control and environmental research. *International Journal of Mass Spectrometry and Ion Processes* **1998**, *173* (3), 191−241.
(41) Hansel, A.; Scholz, W.; Mentler, B.; Fischer, L.; Berndt, T. Detection of RO_2 radicals and other products from cyclohexene ozonolysis with NH_4^+ and acetate chemical ionization mass spectrometry. *Atmos. Environ.* **2018**, *186*, 248−255.
(42) Pankow, J. F.; Asher, W. E. SIMPOL.1: a simple group contribution method for predicting vapor pressures and enthalpies of vaporization of multifunctional organic compounds. *Atmospheric Chemistry and Physics* **2008**, *8* (10), 2773−2796.
(43) Donahue, N. M.; Epstein, S. A.; Pandis, S. N.; Robinson, A. L. A two-dimensional volatility basis set: 1. organic-aerosol mixing thermodynamics. *Atmospheric Chemistry and Physics* **2011**, *11* (7), 3303−3318.
(44) Li, Y.; Pöschl, U.; Shiraiwa, M. Molecular corridors and parameterizations of volatility in the chemical evolution of organic aerosols. *Atmospheric Chemistry and Physics* **2016**, *16* (5), 3327−3344.
(45) Isaacman-VanWertz, G.; Aumont, B. Impact of organic molecular structure on the estimation of atmospherically relevant physicochemical parameters. *Atmospheric Chemistry and Physics* **2021**, *21* (8), 6541−6563.
(46) Daumit, K. E.; Kessler, S. H.; Kroll, J. H. Average chemical properties and potential formation pathways of highly oxidized organic aerosol. *Faraday Discuss.* **2013**, *165*, 181−202.
(47) Wolfe, G. M.; Marvin, M. R.; Roberts, S. J.; Travis, K. R.; Liao, J. The Framework for 0-D Atmospheric Modeling (F0AM) v3.1. *Geoscientific Model Development* **2016**, *9* (9), 3309−3319.
(48) Jenkin, M. E.; Saunders, S. M.; Pilling, M. J. The tropospheric degradation of volatile organic compounds: a protocol for mechanism development. *Atmos. Environ.* **1997**, *31* (1), 81−104.
(49) Kanakidou, M.; Seinfeld, J. H.; Pandis, S. N.; Barnes, I.; Dentener, F. J.; Facchini, M. C.; Van Dingenen, R.; Ervens, B.; Nenes, A.; Nielsen, C. J.; Swietlicki, E.; Putaud, J. P.; Balkanski, Y.; Fuzzi, S.; Horth, J.; Moortgat, G. K.; Winterhalter, R.; Myhre, C. E. L.; Tsigaridis, K.; Vignati, E.; Stephanou, E. G.; Wilson, J. Organic aerosol and global climate modelling: a review. *Atmospheric Chemistry and Physics* **2005**, *5* (4), 1053−1123.
(50) Yan, C.; Nie, W.; Vogel, A. L.; Dada, L.; Lehtipalo, K.; Stolzenburg, D.; Wagner, R.; Rissanen, M. P.; Xiao, M.; Ahonen, L.; Fischer, L.; Rose, C.; Bianchi, F.; Gordon, H.; Simon, M.; Heinritzi, M.; Garmash, O.; Roldin, P.; Dias, A.; Ye, P.; Hofbauer, V.; Amorim, A.; Bauer, P. S.; Bergen, A.; Bernhammer, A.-K.; Breitenlechner, M.; Brilke, S.; Buchholz, A.; Mazon, S. B.; Canagaratna, M. R.; Chen, X.; Ding, A.; Dommen, J.; Draper, D. C.; Duplissy, J.; Frege, C.; Heyn, C.; Guida, R.; Hakala, J.; Heikkinen, L.; Hoyle, C. R.; Jokinen, T.; Kangasluoma, J.; Kirkby, J.; Kontkanen, J.; Kürten, A.; Lawler, M. J.; Mai, H.; Mathot, S.; Mauldin, R. L.; Molteni, U.; Nichman, L.; Nieminen, T.; Nowak, J.; Ojdanic, A.; Onnela, A.; Pajunoja, A.; Petäjä, T.; Piel, F.; Quéléver, L. L. J.; Sarnela, N.; Schallhart, S.; Sengupta, K.; Sipilä, M.; Tomé, A.; Tröstl, J.; Väisänen, O.; Wagner, A. C.; Ylisirniö, A.; Zha, Q.; Baltensperger, U.; Carslaw, K. S.; Curtius, J.; Flagan, R. C.; Hansel, A.; Riipinen, I.; Smith, J. N.; Virtanen, A.; Winkler, P. M.; Donahue, N. M.; Kerminen, V.-M.; Kulmala, M.; Ehn, M.; Worsnop, D. R. Size-dependent influence of NO_x on the growth rates of organic aerosol particles. *Sci. Adv.* **2020**, *6* (22), No. eaay4945.
(51) Lehtipalo, K.; Yan, C.; Dada, L.; Bianchi, F.; Xiao, M.; Wagner, R.; Stolzenburg, D.; Ahonen, L. R.; Amorim, A.; Baccarini, A.; Bauer, P. S.; Baumgartner, B.; Bergen, A.; Bernhammer, A.-K.; Breitenlechner, M.; Brilke, S.; Buchholz, A.; Mazon, S. B.; Chen, D.; Chen, X.; Dias, A.; Dommen, J.; Draper, D. C.; Duplissy, J.; Ehn, M.; Finkenzeller, H.; Fischer, L.; Frege, C.; Fuchs, C.; Garmash, O.; Gordon, H.; Hakala, J.; He, X.; Heikkinen, L.; Heinritzi, M.; Helm, J. C.; Hofbauer, V.; Hoyle, C. R.; Jokinen, T.; Kangasluoma, J.; Kerminen, V.-M.; Kim, C.; Kirkby, J.; Kontkanen, J.; Kürten, A.; Lawler, M. J.; Mai, H.; Mathot, S.; Mauldin, R. L.; Molteni, U.; Nichman, L.; Nie, W.; Nieminen, T.; Ojdanic, A.; Onnela, A.; Passananti, M.; Petäjä, T.; Piel, F.; Pospisilova, V.; Quéléver, L. L. J.; Rissanen, M. P.; Rose, C.; Sarnela, N.; Schallhart, S.; Schuchmann, S.; Sengupta, K.; Simon, M.; Sipilä, M.; Tauber, C.; Tomé, A.; Tröstl, J.; Väisänen, O.; Vogel, A. L.; Volkamer, R.; Wagner, A. C.; Wang, M.; Weitz, L.; Wimmer, D.; Ye, P.; Ylisirniö, A.; Zha, Q.; Carslaw, K. S.; Curtius, J.; Donahue, N. M.; Flagan, R. C.; Hansel, A.; Riipinen, I.; Virtanen, A.; Winkler, P. M.; Baltensperger, U.; Kulmala, M.; Worsnop, D. R. Multicomponent new particle formation from sulfuric acid, ammonia, and biogenic vapors. *Sci. Adv.* **2018**, *4* (12), No. eaau5363.
(52) McFiggans, G.; Mentel, T. F.; Wildt, J.; Pullinen, I.; Kang, S.; Kleist, E.; Schmitt, S.; Springer, M.; Tillmann, R.; Wu, C.; Zhao, D.; Hallquist, M.; Faxon, C.; Le Breton, M.; Hallquist, A. M.; Simpson, D.; Bergstrom, R.; Jenkin, M. E.; Ehn, M.; Thornton, J. A.; Alfarra, M. R.; Bannan, T. J.; Percival, C. J.; Priestley, M.; Topping, D.; Kiendler-Scharr, A. Secondary organic aerosol reduced by mixture of atmospheric vapours. *Nature* **2019**, *565* (7741), 587−593.
(53) Heinritzi, M.; Dada, L.; Simon, M.; Stolzenburg, D.; Wagner, A. C.; Fischer, L.; Ahonen, L. R.; Amanatidis, S.; Baalbaki, R.; Baccarini, A.; Bauer, P. S.; Baumgartner, B.; Bianchi, F.; Brilke, S.; Chen, D.; Chiu, R.; Dias, A.; Dommen, J.; Duplissy, J.; Finkenzeller, H.; Frege, C.; Fuchs, C.; Garmash, O.; Gordon, H.; Granzin, M.; El Haddad, I.; He, X.; Helm, J.; Hofbauer, V.; Hoyle, C. R.; Kangasluoma, J.; Keber, T.; Kim, C.; Kürten, A.; Lamkaddam, H.; Laurila, T. M.; Lampilahti, J.; Lee, C. P.; Lehtipalo, K.; Leiminger, M.; Mai, H.; Makhmutov, V.; Manninen, H. E.; Marten, R.; Mathot, S.; Mauldin, R. L.; Mentler, B.; Molteni, U.; Müller, T.; Nie, W.; Nieminen, T.; Onnela, A.; Partoll, E.; Passananti, M.; Petäjä, T.; Pfeifer, J.; Pospisilova, V.; Quéléver, L. L. J.; Rissanen, M. P.; Rose, C.; Schobesberger, S.; Scholz, W.; Scholze, K.; Sipilä, M.; Steiner, G.; Stozhkov, Y.; Tauber, C.; Tham, Y. J.; Vazquez-Pufleau, M.; Virtanen, A.; Vogel, A. L.; Volkamer, R.; Wagner, R.; Wang, M.; Weitz, L.; Wimmer, D.; Xiao, M.; Yan, C.; Ye, P.; Zha, Q.; Zhou, X.; Amorim, A.; Baltensperger, U.; Hansel, A.; Kulmala, M.; Tomé, A.; Winkler, P. M.; Worsnop, D. R.; Donahue, N. M.; Kirkby, J.; Curtius, J. Molecular understanding of the suppression of new-particle formation by isoprene. *Atmospheric Chemistry and Physics* **2020**, *20* (20), 11809−11821.
(54) Berndt, T.; Richters, S.; Jokinen, T.; Hyttinen, N.; Kurten, T.; Otkjaer, R. V.; Kjaergaard, H. G.; Stratmann, F.; Herrmann, H.; Sipila, M.; Kulmala, M.; Ehn, M. Hydroxyl radical-induced formation of highly oxidized organic compounds. *Nat. Commun.* **2016**, *7*, 13677.
(55) Kurtén, T.; Møller, K. H.; Nguyen, T. B.; Schwantes, R. H.; Misztal, P. K.; Su, L.; Wennberg, P. O.; Fry, J. L.; Kjaergaard, H. G. Alkoxy Radical Bond Scissions Explain the Anomalously Low Secondary Organic Aerosol and Organonitrate Yields From alpha-Pinene + NO_3. *J. Phys. Chem. Lett.* **2017**, *8* (13), 2826−2834.
(56) Lopez-Hilfiker, F. D.; Mohr, C.; Ehn, M.; Rubach, F.; Kleist, E.; Wildt, J.; Mentel, T. F.; Lutz, A.; Hallquist, M.; Worsnop, D.; Thornton, J. A. A novel method for online analysis of gas and particle composition: description and evaluation of a Filter Inlet for Gases and AEROsols (FIGAERO). *Atmospheric Measurement Techniques* **2014**, *7* (4), 983−1001.

https://doi.org/10.1021/acs.est.3c07958
Environ. Sci. Technol. 2024, 58, 1601−1614

(57) Huang, W.; Saathoff, H.; Pajunoja, A.; Shen, X.; Naumann, K. H.; Wagner, R.; Virtanen, A.; Leisner, T.; Mohr, C. α-Pinene secondary organic aerosol at low temperature: chemical composition and implications for particle viscosity. *Atmospheric Chemistry and Physics* **2018**, *18* (4), 2883−2898.
(58) Wang, D. S.; Hildebrandt Ruiz, L. Chlorine-initiated oxidation of n-alkanes under high-NO_x conditions: insights into secondary organic aerosol composition and volatility using a FIGAERO−CIMS. *Atmospheric Chemistry and Physics* **2018**, *18* (21), 15535−15553.
(59) Wang, M.; Chen, D.; Xiao, M.; Ye, Q.; Stolzenburg, D.; Hofbauer, V.; Ye, P.; Vogel, A. L.; Mauldin, R. L., 3rd; Amorim, A.; Baccarini, A.; Baumgartner, B.; Brilke, S.; Dada, L.; Dias, A.; Duplissy, J.; Finkenzeller, H.; Garmash, O.; He, X. C.; Hoyle, C. R.; Kim, C.; Kvashnin, A.; Lehtipalo, K.; Fischer, L.; Molteni, U.; Petaja, T.; Pospisilova, V.; Quelever, L. L. J.; Rissanen, M.; Simon, M.; Tauber, C.; Tome, A.; Wagner, A. C.; Weitz, L.; Volkamer, R.; Winkler, P. M.; Kirkby, J.; Worsnop, D. R.; Kulmala, M.; Baltensperger, U.; Dommen, J.; El-Haddad, I.; Donahue, N. M. Photo-oxidation of Aromatic Hydrocarbons Produces Low-Volatility Organic Compounds. *Environ. Sci. Technol.* **2020**, *54* (13), 7911−7921.
(60) Stolzenburg, D.; Fischer, L.; Vogel, A. L.; Heinritzi, M.; Schervish, M.; Simon, M.; Wagner, A. C.; Dada, L.; Ahonen, L. R.; Amorim, A.; Baccarini, A.; Bauer, P. S.; Baumgartner, B.; Bergen, A.; Bianchi, F.; Breitenlechner, M.; Brilke, S.; Mazon, S. B.; Chen, D.; Dias, A.; Draper, D. C.; Duplissy, J.; Haddad, I. E.; Finkenzeller, H.; Frege, C.; Fuchs, C.; Garmash, O.; Gordon, H.; He, X.; Helm, J.; Hofbauer, V.; Hoyle, C. R.; Kim, C.; Kirkby, J.; Kontkanen, J.; Kürten, A.; Lampilahti, J.; Lawler, M.; Lehtipalo, K.; Leiminger, M.; Mai, H.; Mathot, S.; Mentler, B.; Molteni, U.; Nie, W.; Nieminen, T.; Nowak, J. B.; Ojdanic, A.; Onnela, A.; Passananti, M.; Petäjä, T.; Quéléver, L. L. J.; Rissanen, M. P.; Sarnela, N.; Schallhart, S.; Tauber, C.; Tomé, A.; Wagner, R.; Wang, M.; Weitz, L.; Wimmer, D.; Xiao, M.; Yan, C.; Ye, P.; Zha, Q.; Baltensperger, U.; Curtius, J.; Dommen, J.; Flagan, R. C.; Kulmala, M.; Smith, J. N.; Worsnop, D. R.; Hansel, A.; Donahue, N. M.; Winkler, P. M. Rapid growth of organic aerosol nanoparticles over a wide tropospheric temperature range. *Proc. Natl. Acad. Sci. U. S. A.* **2018**, *115* (37), 9122−9127.
(61) Schervish, M.; Donahue, N. M. Peroxy radical chemistry and the volatility basis set. *Atmospheric Chemistry and Physics* **2020**, *20* (2), 1183−1199.
(62) Donahue, N. M.; Kroll, J. H.; Pandis, S. N.; Robinson, A. L. A two-dimensional volatility basis set − Part 2: Diagnostics of organic-aerosol evolution. *Atmospheric Chemistry and Physics* **2012**, *12* (2), 615−634.
(63) Simon, M.; Dada, L.; Heinritzi, M.; Scholz, W.; Stolzenburg, D.; Fischer, L.; Wagner, A. C.; Kürten, L.; Rörup, B.; He, X.-C.; Almeida, J.; Baalbaki, R.; Baccarini, A.; Bauer, P. S.; Beck, L.; Bergen, A.; Bianchi, F.; Bräkling, S.; Brilke, S.; Caudillo, L.; Chen, D.; Chu, B.; Dias, A.; Draper, D. C.; Duplissy, J.; El-Haddad, I.; Finkenzeller, H.; Frege, C.; Gonzalez-Carracedo, L.; Gordon, H.; Granzin, M.; Hakala, J.; Hofbauer, V.; Hoyle, C. R.; Kim, C.; Kong, W.; Lamkaddam, H.; Lee, C. P.; Lehtipalo, K.; Leiminger, M.; Mai, H.; Manninen, H. E.; Marie, G.; Marten, R.; Mentler, B.; Molteni, U.; Nichman, L.; Nie, W.; Ojdanic, A.; Onnela, A.; Partoll, E.; Petäjä, T.; Pfeifer, J.; Philippov, M.; Quéléver, L. L. J.; Ranjithkumar, A.; Rissanen, M. P.; Schallhart, S.; Schobesberger, S.; Schuchmann, S.; Shen, J.; Sipilä, M.; Steiner, G.; Stozhkov, Y.; Tauber, C.; Tham, Y. J.; Tomé, A. R.; Vazquez-Pufleau, M.; Vogel, A. L.; Wagner, R.; Wang, M.; Wang, D. S.; Wang, Y.; Weber, S. K.; Wu, Y.; Xiao, M.; Yan, C.; Ye, P.; Ye, Q.; Zauner-Wieczorek, M.; Zhou, X.; Baltensperger, U.; Dommen, J.; Flagan, R. C.; Hansel, A.; Kulmala, M.; Volkamer, R.; Winkler, P. M.; Worsnop, D. R.; Donahue, N. M.; Kirkby, J.; Curtius, J. Molecular understanding of new-particle formation from α-pinene between − 50 and + 25 °C. *Atmospheric Chemistry and Physics* **2020**, *20* (15), 9183−9207.
(64) Junninen, H.; Ahonen, L.; Bianchi, F.; Quéléver, L.; Schallhart, S.; Dada, L.; Manninen, H. E.; Leino, K.; Lampilahti, J.; Buenrostro Mazon, S.; Rantala, P.; Räty, M.; Kontkanen, J.; Negri, S.; Aliaga, D.; Garmash, O.; Alekseychik, P.; Lipp, H.; Tamme, K.; Levula, J.; Sipilä, M.; Ehn, M.; Worsnop, D.; Zilitinkevich, S.; Mammarella, I.; Rinne, J.; Vesala, T.; Petäjä, T.; Kerminen, V.-M.; Kulmala, M. Terpene emissions from boreal wetlands can initiate stronger atmospheric new particle formation than boreal forests. *Commun. Earth Environ.* **2022**, *3* (1), 93.
(65) Junninen, H.; Ahonen, L.; Bianchi, F.; Quéléver, L.; Schallhart, S.; Dada, L.; Manninen, H. E.; Leino, K.; Lampilahti, J.; Buenrostro Mazon, S.; Rantala, P.; Räty, M.; Kontkanen, J.; Negri, S.; Aliaga, D.; Garmash, O.; Alekseychik, P.; Lipp, H.; Tamme, K.; Levula, J.; Sipilä, M.; Ehn, M.; Worsnop, D.; Zilitinkevich, S.; Mammarella, I.; Rinne, J.; Vesala, T.; Petäjä, T.; Kerminen, V.-M.; Kulmala, M. Terpene emissions from boreal wetlands can initiate stronger atmospheric new particle formation than boreal forests. *Commun. Earth Environ.* **2022**, *3* (1), 93 DOI: 10.1038/s43247-022-00406-9.
(66) Vettikkat, L.; Miettinen, P.; Buchholz, A.; Rantala, P.; Yu, H.; Schallhart, S.; Petäjä, T.; Seco, R.; Männistö, E.; Kulmala, M.; Tuittila, E. S.; Guenther, A. B.; Schobesberger, S. High emission rates and strong temperature response make boreal wetlands a large source of isoprene and terpenes. *Atmospheric Chemistry and Physics* **2023**, *23* (4), 2683−2698.
(67) Shen, H.; Zhao, D.; Pullinen, I.; Kang, S.; Vereecken, L.; Fuchs, H.; Acir, I.-H.; Tillmann, R.; Rohrer, F.; Wildt, J.; Kiendler-Scharr, A.; Wahner, A.; Mentel, T. F. Highly Oxygenated Organic Nitrates Formed from NO_3 Radical-Initiated Oxidation of β-Pinene. *Environ. Sci. Technol.* **2021**, *55* (23), 15658−15671.
(68) Guo, Y.; Shen, H.; Pullinen, I.; Luo, H.; Kang, S.; Vereecken, L.; Fuchs, H.; Hallquist, M.; Acir, I. H.; Tillmann, R.; Rohrer, F.; Wildt, J.; Kiendler-Scharr, A.; Wahner, A.; Zhao, D.; Mentel, T. F. Identification of highly oxygenated organic molecules and their role in aerosol formation in the reaction of limonene with nitrate radical. *Atmospheric Chemistry and Physics* **2022**, *22* (17), 11323−11346.
(69) Huang, W.; Saathoff, H.; Shen, X.; Ramisetty, R.; Leisner, T.; Mohr, C. Chemical Characterization of Highly Functionalized Organonitrates Contributing to Night-Time Organic Aerosol Mass Loadings and Particle Growth. *Environ. Sci. Technol.* **2019**, *53* (3), 1165−1174.

Nitrate radicals suppress biogenic new particle formation from monoterpene oxidation

Dandan Li[1,†], Wei Huang[2,†], Dongyu Wang[3], Mingyi Wang[4,§], Joel A. Thornton[5], Lucía Caudillo[6], Birte Rörup[2], Ruby Marten[3], Wiebke Scholz[7], Henning Finkenzeller[8], Guillaume Marie[6], Urs Baltensperger[3], David M. Bell[3], Zoé Brasseur[2], Joachim Curtius[6], Lubna Dada[3], Jonathan Duplissy[2,9], Xianda Gong[10], Armin Hansel[7], Xu-Cheng He[2], Victoria Hofbauer[4], Heikki Junninen[11], Jordan E. Krechmer[12], Andreas Kürten[6], Houssni Lamkaddam[3], Katrianne Lehtipalo[2,13], Brandon Lopez[4], Yingge Ma[14], Naser G. A. Mahfouz[15], Hanna E. Manninen[16], Bernhard Mentler[7], Sebastien Perrier[1], Tuukka Petäjä[2], Joschka Pfeifer[16], Maxim Philippov[17], Meredith Schervish[4], Siegfried Schobesberger[18], Jiali Shen[2], Mihnea Surdu[3], Sophie Tomaz[1], Rainer Volkamer[8], Xinke Wang[1], Stefan K. Weber[6,16], André Welti[13], Douglas R. Worsnop[2,12], YushengWu[2], Chao Yan[2], Marcel Zauner-Wieczorek[6], Markku Kulmala[2], Jasper Kirkby[6,16], Neil M. Donahue[4], Christian George[1], Imad El-Haddad[3,], Federico Bianchi[2,*], Matthieu Riva[1,*]*

[1] Univ Lyon, Université Claude Bernard Lyon 1, CNRS, IRCELYON, 69626, Villeurbanne, France

[2] Institute for Atmospheric and Earth System Research/Physics, Faculty of Science, University of Helsinki, 00014, Helsinki, Finland

[3] Laboratory of Atmospheric Chemistry, Paul Scherrer Institute, 5232, Villigen, Switzerland

[4] Center for Atmospheric Particle Studies, Carnegie Mellon University, Pittsburgh, PA, 15213, USA

[5] Department of Atmospheric Sciences, University of Washington, Seattle, WA 98195, USA

[6] Institute for Atmospheric and Environmental Sciences, Goethe University Frankfurt, 60438, Frankfurt am Main, Germany

[7] Institute for Ion Physics and Applied Physics, University of Innsbruck, 6020, Innsbruck, Austria

[8] Department of Chemistry & CIRES, University of Colorado Boulder, Boulder, CO 80309, USA

[9] Helsinki Institute of Physics (HIP)/Physics, Faculty of Science, University of Helsinki, 00014, Helsinki, Finland

[10] Leibniz Institute for Tropospheric Research, 04318, Leipzig, Germany

[11] Institute of Physics, University of Tartu, 50090, Tartu, Estonia

[12] Aerodyne Research Inc., Billerica, Massachusetts 01821, USA

[13] Finnish Meteorological Institute, 00560, Helsinki, Finland

[14] State Environmental Protection Key Laboratory of Formation and Prevention of Urban Air Pollution Complex, Shanghai Academy of Environment Sciences, 200233, Shanghai, P. R. China

[15] Atmospheric and Oceanic Sciences, Princeton University, Princeton, NJ 08540, USA

[16] CERN, the European Organization for Nuclear Research, CH-1211 Geneve 23, Switzerland

[17] P.N. Lebedev Physical Institute of the Russian Academy of Sciences, 119991, Moscow, Russia

[18] Department of Applied Physics, University of Eastern Finland, 70211, Kuopio, Finland

This PDF file includes:

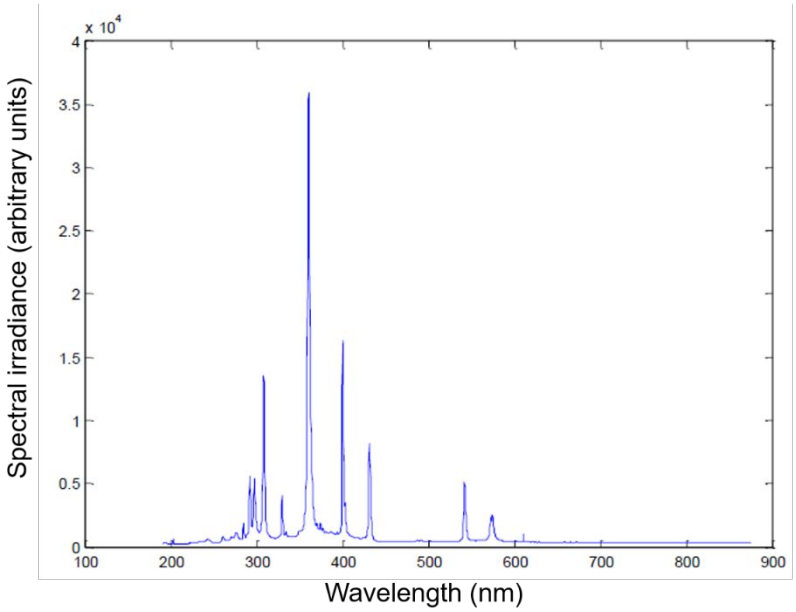

Figure S1. Spectrum of mercury-doped xenon arc lamps (UVH) in the CLOUD chamber. Four 200 W Hamamatsu Hg-Xe lamps (UVH) provide light across the entire UV-Vis spectral range and illuminate the chamber homogeneously.

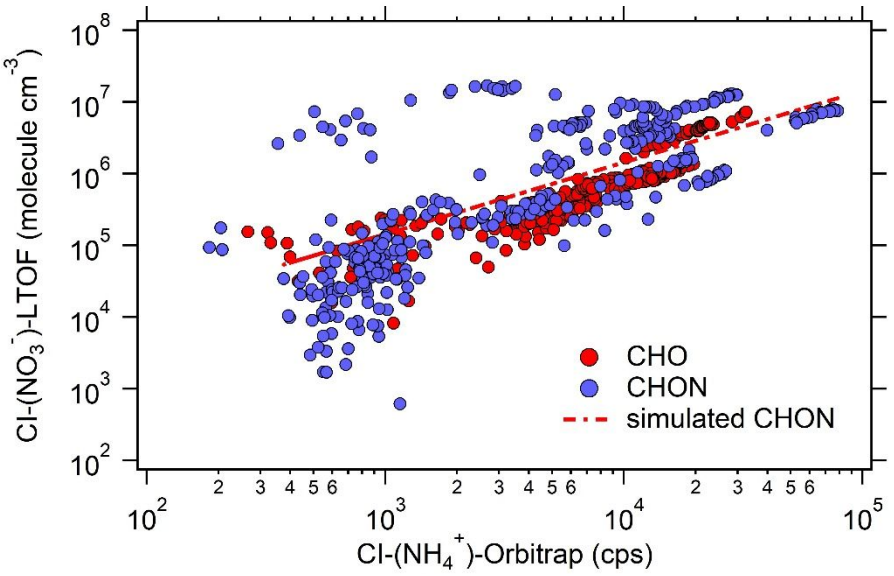

Figure S2. Sensitivity of CI-(NH_4^+)-Orbitrap for the detection of CHO and CHON in the CLOUD chamber. Time evolution intercomparison of CHO (red marker) and CHON (blue marker) measured by CI-(NH_4^+)-Orbitrap and CI-(NO_3^-)-LTOF. Time evolution of CHO species with correlation coefficients $R^2 > 0.9$ between NH_4^+-Orbitrap (cps in unit) and NO_3^--LTOF (molecule cm^{-3} in unit) are used to obtain the calibration factor applied to estimate the concentration of CHON measured by NH_4^+-Orbitrap (red dashed line). The outliers for CHON measured by CI-(NO_3^-)-LTOF is the time evolution of one compound ($C_{10}H_{15}NO_{10}$).

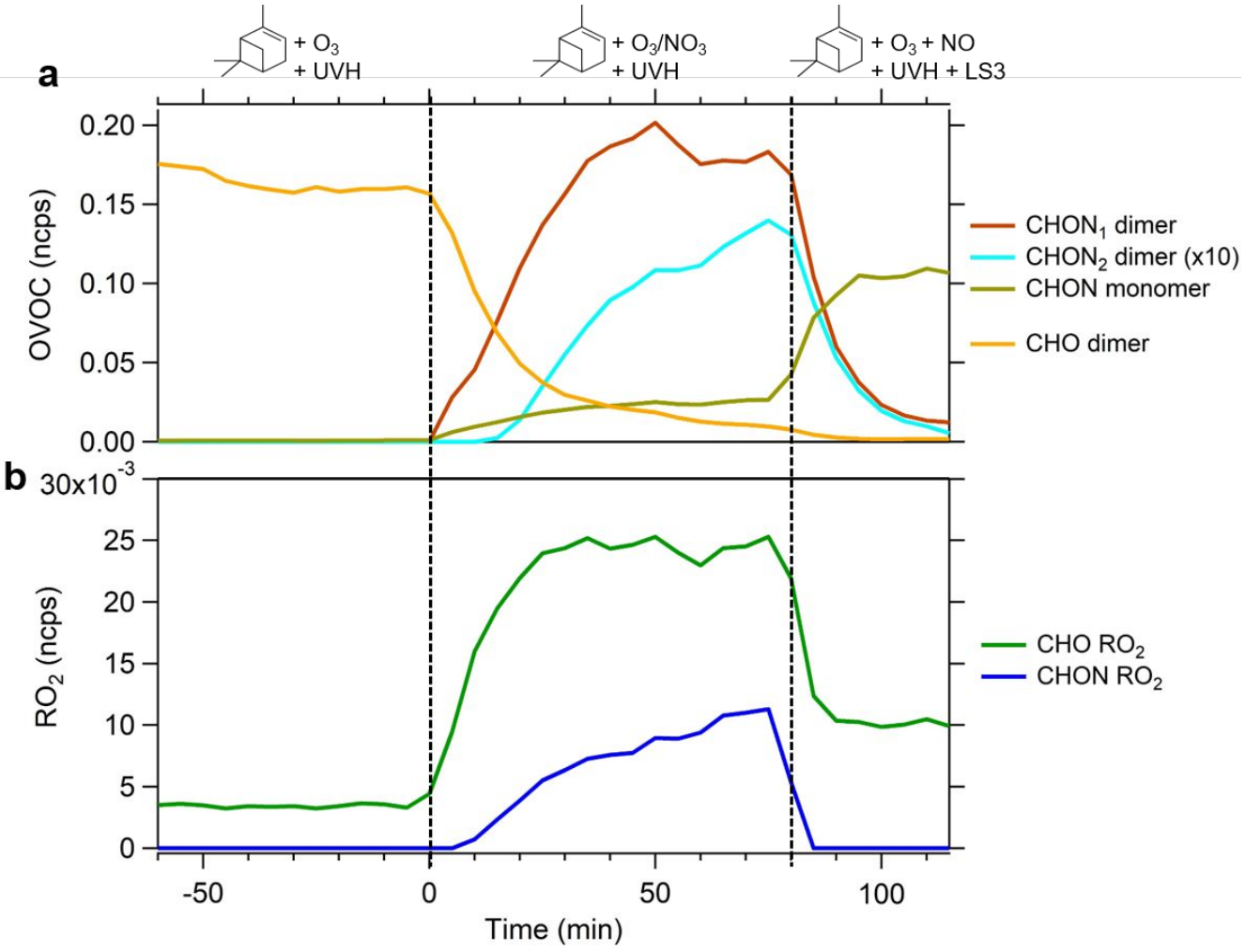

Figure S3. Effect of NO_3 radicals and NO on OVOC in CLOUD. Evolution of 1 N-containing dimers ($CHON_1$ dimer), 2 N-containing dimers ($CHON_2$ dimer), N-containing monomers (CHON monomer) and non-N containing dimer (CHO dimer) **(a)** and N-containing RO_2 radicals (CHON RO_2) and non-N containing RO_2 radicals (CHO RO_2) **(b)**.

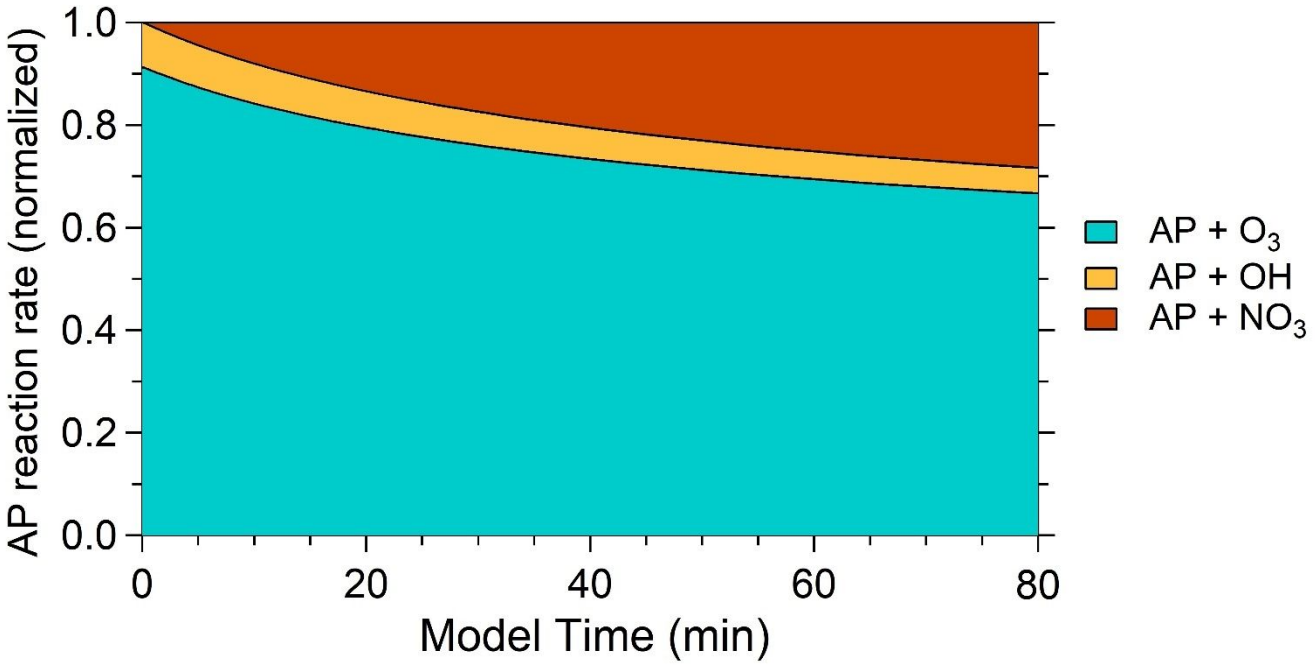

Figure S4. Evolution of normalized α-pinene reaction rate during the NO_3 perturbed ozonolysis stage in CLOUD chamber. The contributions of different oxidants to the reacted α-pinene were simulated using F0AM model when NO_3 was present in the chamber during t = 0-80 mins.

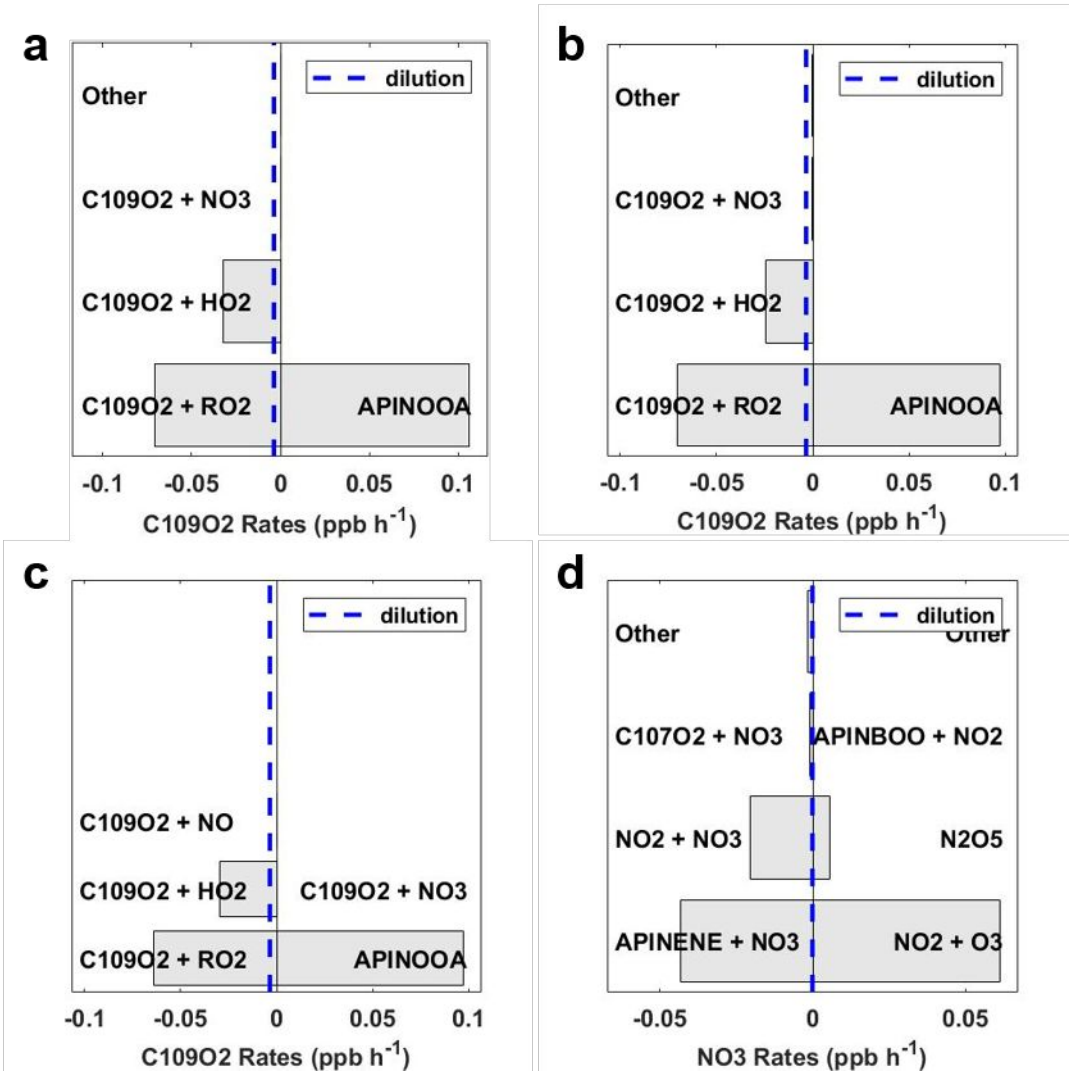

Figure S5. Fate of $C_{10}H_{15}O_4$ and NO_3 radicals simulated in CLOUD chamber. Production and loss rates of $C_{10}H_{15}O_4$ (C109O2) radical during pure ozonolysis **(a)**, during ozonolysis perturbed by NO_3 **(b)**, and during ozonolysis perturbed by NO_x **(c)**. Production and loss rates of formed NO_3 radical during NO_2 injected into the chamber at t = 0-80 min **(d)**. APINOOA, C107O2 and APINBOO in the figure refer to Criegee Intermediate, $C_{10}H_{15}O_4$ and $C_{10}H_{17}O_3$, respectively.

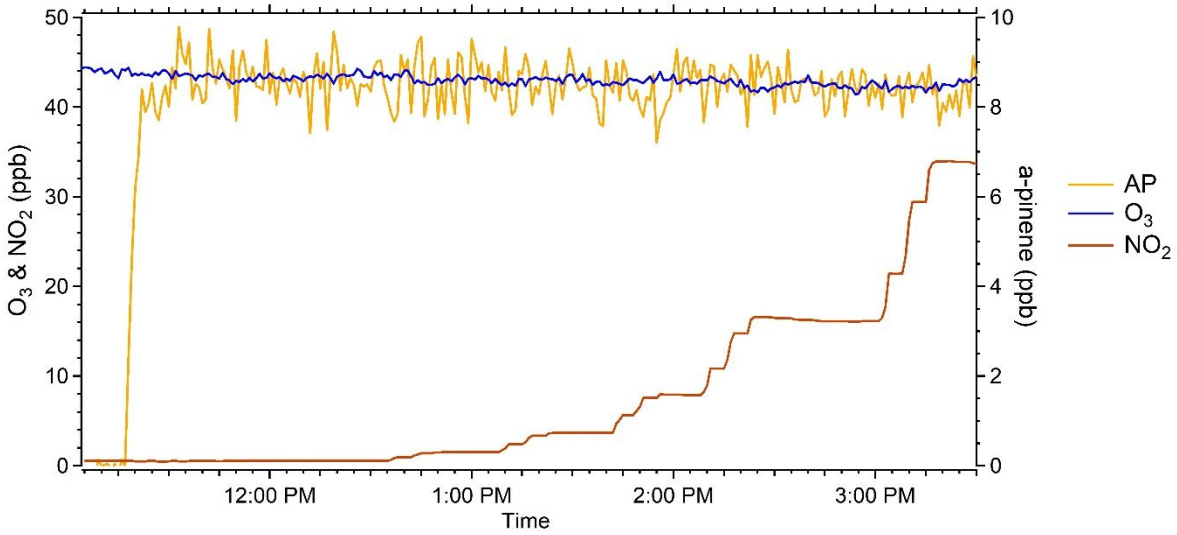

Figure S6. Precursors for oxidation flow reactor (OFR) experiments. A run of the evolution of trace gas α-pinene, O_3, and NO_2 in the OFR outflow. Constant α-pinene and O_3 were injected to the OFR. The concentration of NO_2 in the OFR varied from 0–75 ppbv. Experiments were conducted at 296 K and RH < 1%.

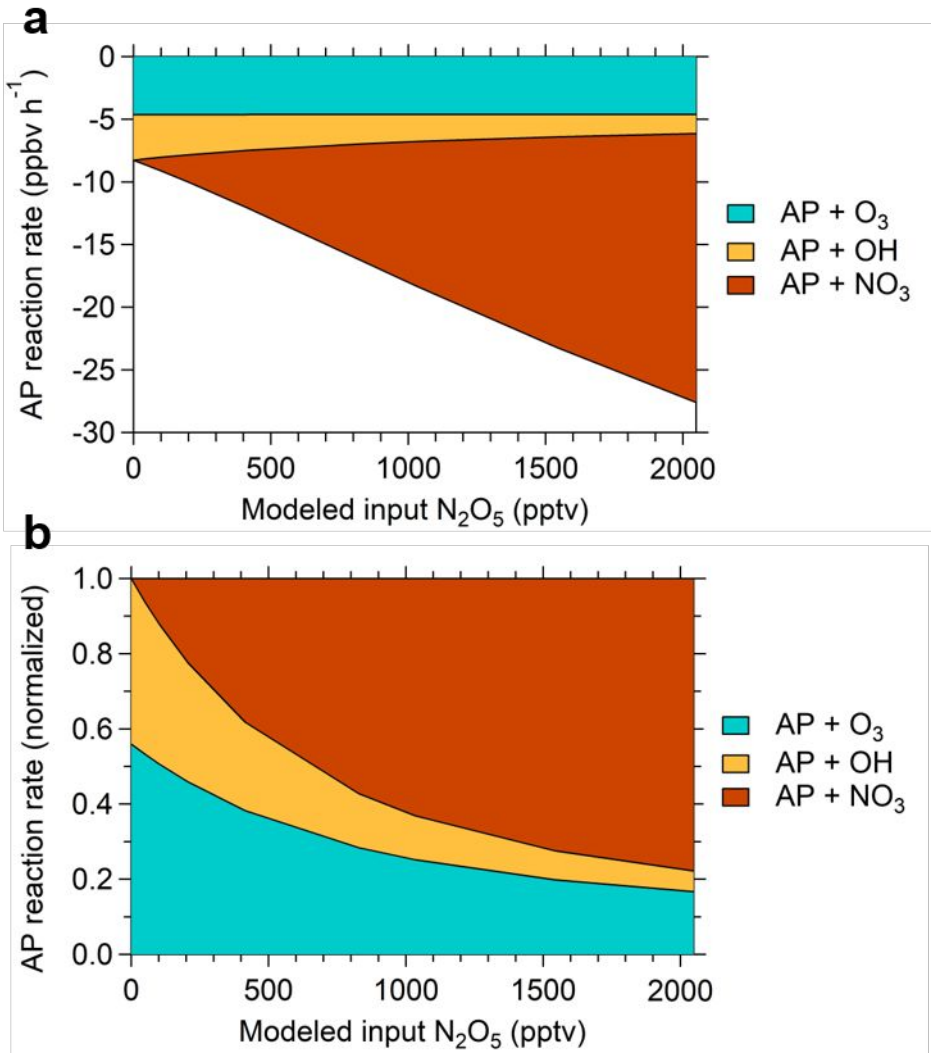

Figure S7. Simulated reactivity of α-pinene at different NO_3 levels in OFR experiments. Absolute reaction rate of α-pinene **(a)** and normalized reaction rate of α-pinene **(b)** as a function of modeled input N_2O_5 concentration. The contributions of different oxidants to the reacted α-pinene at nine NO_3 concentrations were simulated using F0AM model.

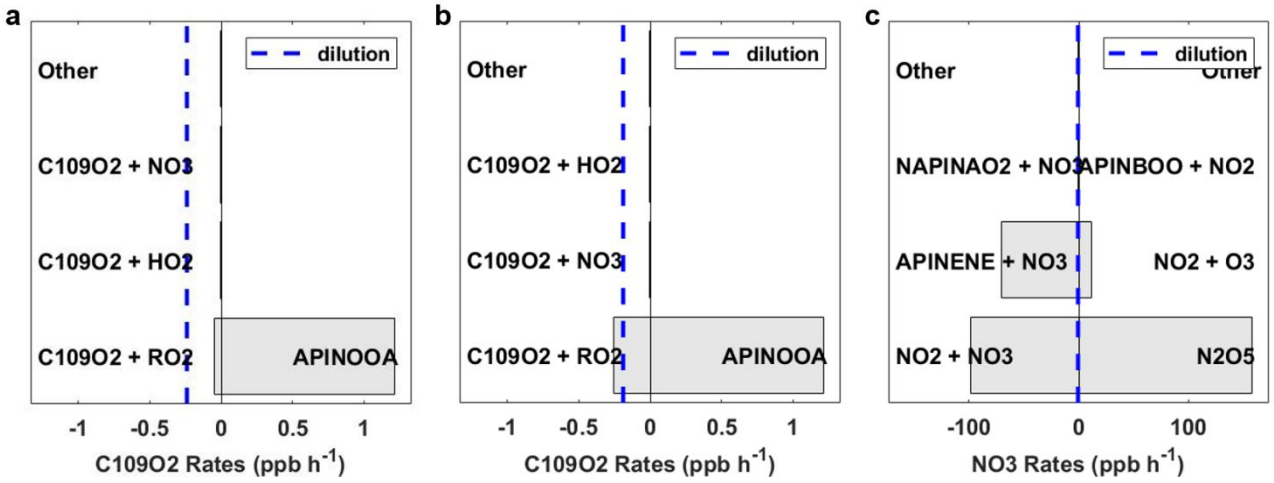

Figure S8. Fate of NO_3 and $C_{10}H_{15}O_4$ radicals simulated in OFR experiments. Production and loss rates of $C_{10}H_{15}O_4$ (C109O2) radicals in O_3/OH chemistry **(a)**, and at highest NO_2:O_3 **(b)**. Production and loss rates of NO_3 at highest NO_2:O_3 **(c)**. The concentration of α-pinene + O_3 were used as input in (a), α-pinene + O_3 + NO_2 in (b) and O_3 + NO_2 in (c). The input concentration of α-pinene, O_3, and NO_2 were 10 ppbv, 50 ppbv, and 75 ppbv, respectively. APINOOA, NAPINAO2 and APINBOO in the figure refer to Criegee Intermediate, $C_{10}H_{16}NO_5$ and $C_{10}H_{17}O_3$, respectively.

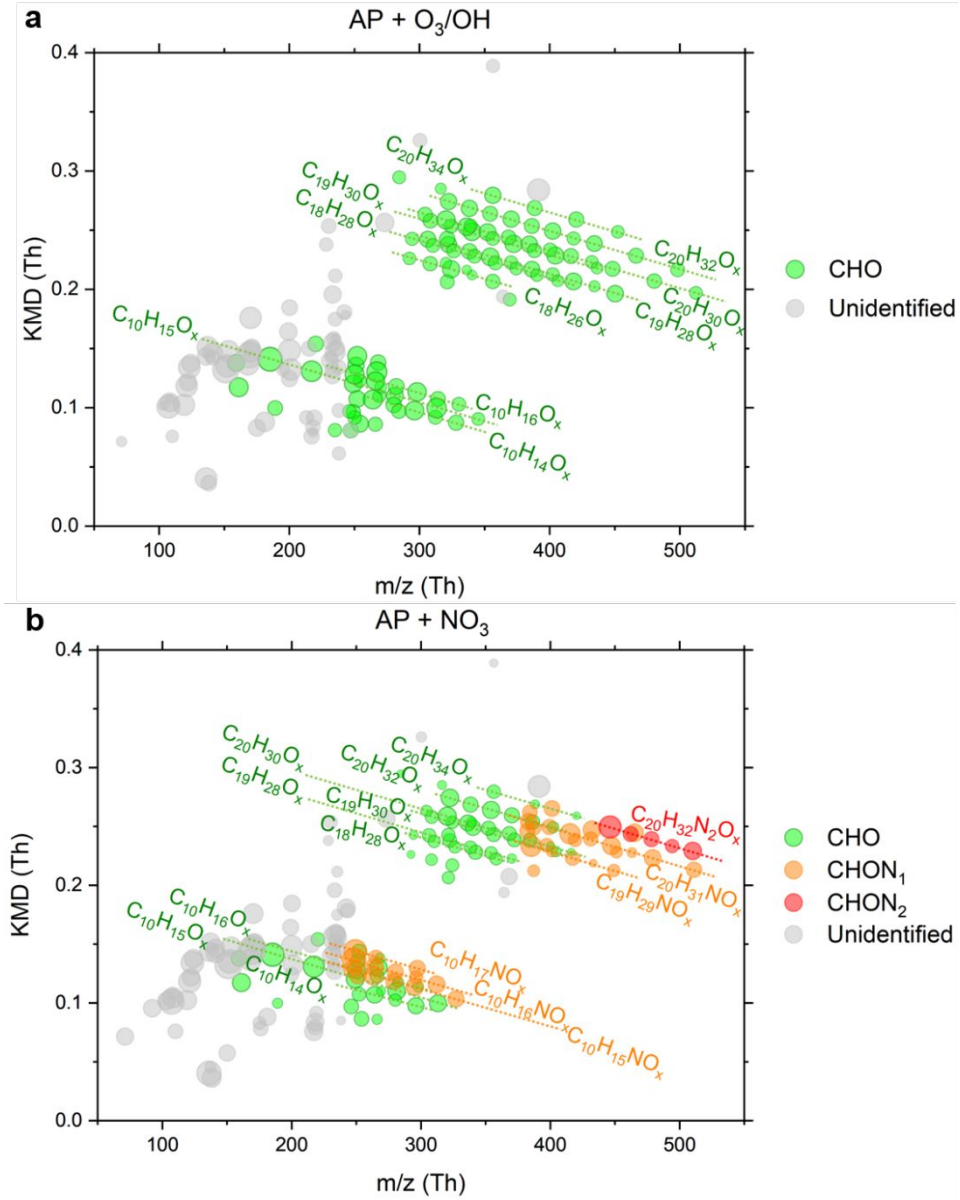

Figure S9. Kendrick mass defect plots of OVOCs in OFR experiments measured by CI-(NH_4^+)-Orbitrap. Kendrick mass defect plots of gaseous compounds observed in the reactions of α-pinene with O_3/OH **(a)** and NO_3 radical at highest NO_2:O_3 **(b)**. The circles are the measured ions colored by groups: CHO, $CHON_1$, $CHON_2$, and unidentified compounds, the sizes of which correspond to their logarithmic intensities. The unidentified compounds represent products with apparent evolution but unassigned molecular formulae.

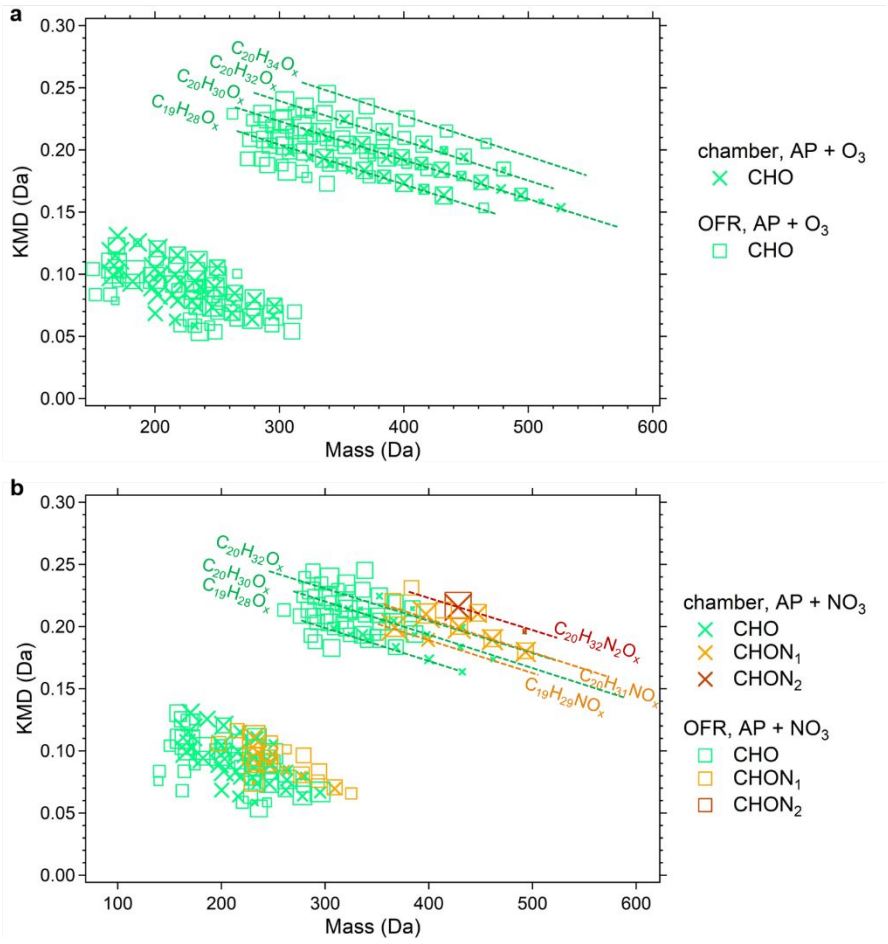

Figure S10. Kendrick mass defect plots of OVOCs observed in the CLOUD chamber and OFR experiments. Mass defect plots for $C_{9\text{-}10}$ monomers and $C_{19\text{-}20}$ dimers from pure ozonolysis in the chamber versus from O_3/OH chemistry in OFR experiments **(a)**. Mass defect plots for $C_{9\text{-}10}$ monomers and $C_{19\text{-}20}$ dimers from ozonolysis perturbed by NO_3 in the chamber versus from OFR at lowest NO_2:O_3 **(b)**. Data at which about 30% of α-pinene was oxidized by NO_3 radicals were used for comparison between CLOUD and OFR experiments. The circles are the measured molecules colored by groups: CHO, $CHON_1$, and $CHON_2$, the sizes of which correspond to their logarithmic intensities. Cross and square markers correspond to chamber and OFR data measured by CI-(NH_4^+)-Orbitrap, respectively. The abscissa represents the measured mass of the compounds which has subtracted the reagent ions.

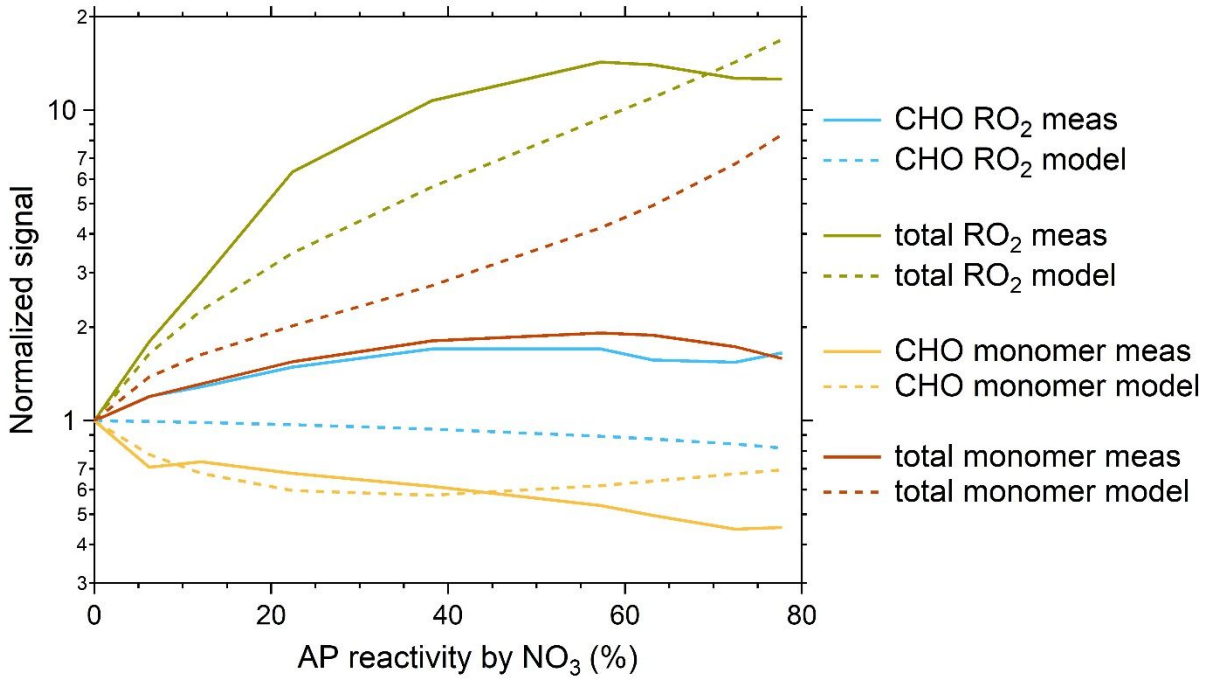

104

105 **Figure S11. Low oxygenated OVOCs measured by CI-(NH_4^+)-Orbitrap and simulated in OFR**
106 **experiments.** Normalized signals of low oxygenated CHO RO_2 (i.e., $C_{10}H_{15}O_4$ from O_3), total RO_2 (CHO
107 RO_2 and $C_{10}H_{16}NO_5$ from NO_3), CHO monomers ($C_{10}H_{14}O_3$, $C_{10}H_{16}O_{2\text{-}4}$, and $C_{10}H_{18}O_3$), and total
108 monomer (CHO monomers, $C_{10}H_{15}NO_4$, and $C_{10}H_{17}NO_{4,5}$) as a function of α-pinene reactivity by NO_3
109 radicals. Results measured by CI-(NH_4^+)-Orbitrap are given in solid lines and those simulated by F0AM
110 in dashed lines.

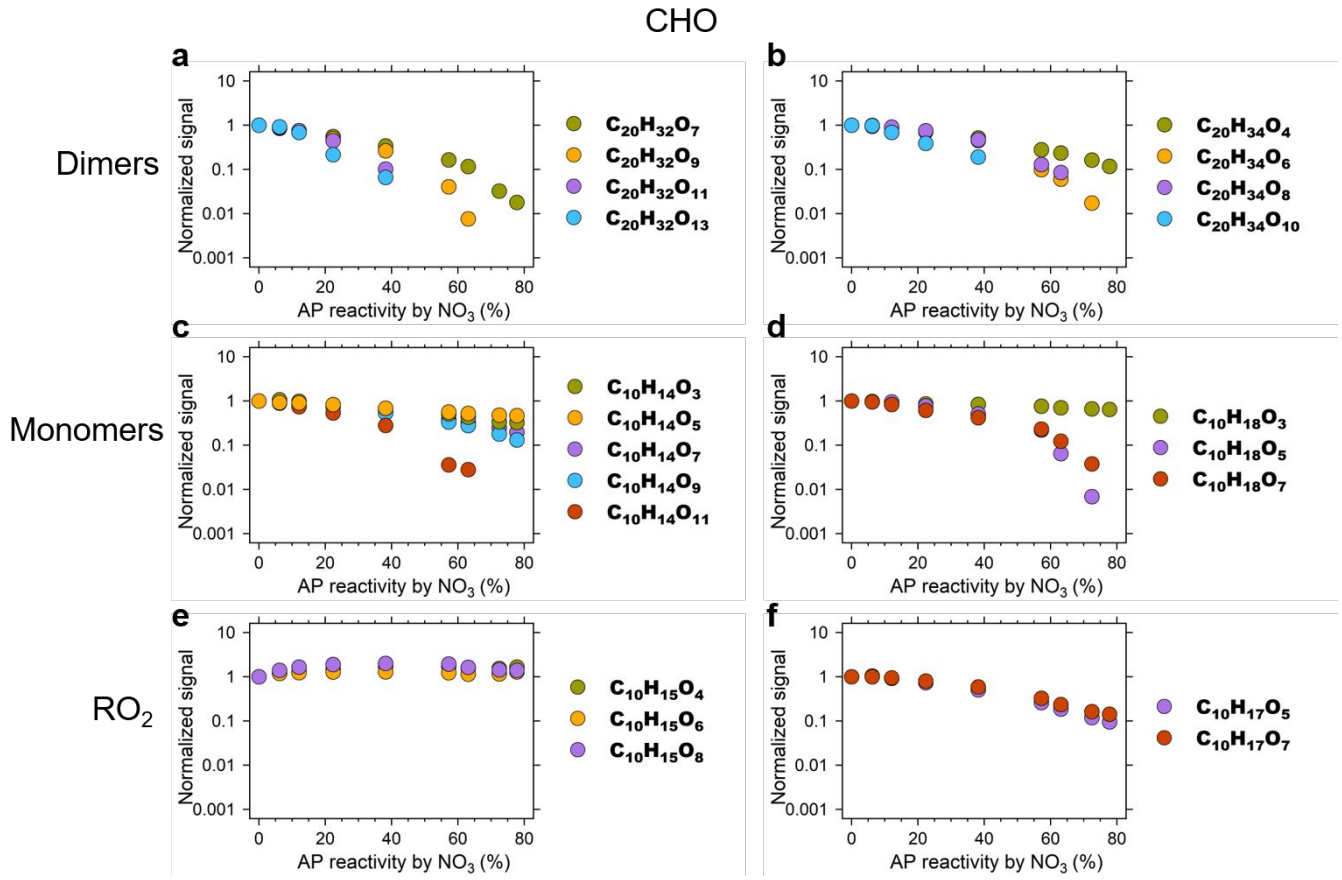

Figure S12. CHO in OFR experiments measured by CI-(NH_4^+)-Orbitrap. Normalized signals of dimers $C_{20}H_{32}O_x$ **(a)** and $C_{20}H_{34}O_x$ **(b)**, monomers $C_{10}H_{14}O_x$ **(c)** and $C_{10}H_{18}O_x$ **(d)**, peroxy radicals $C_{10}H_{15}O_x$ **(e)** and $C_{10}H_{17}O_x$ **(f)** derived from O_3/OH chemistry as a function of α-pinene reactivity by NO_3 radicals.

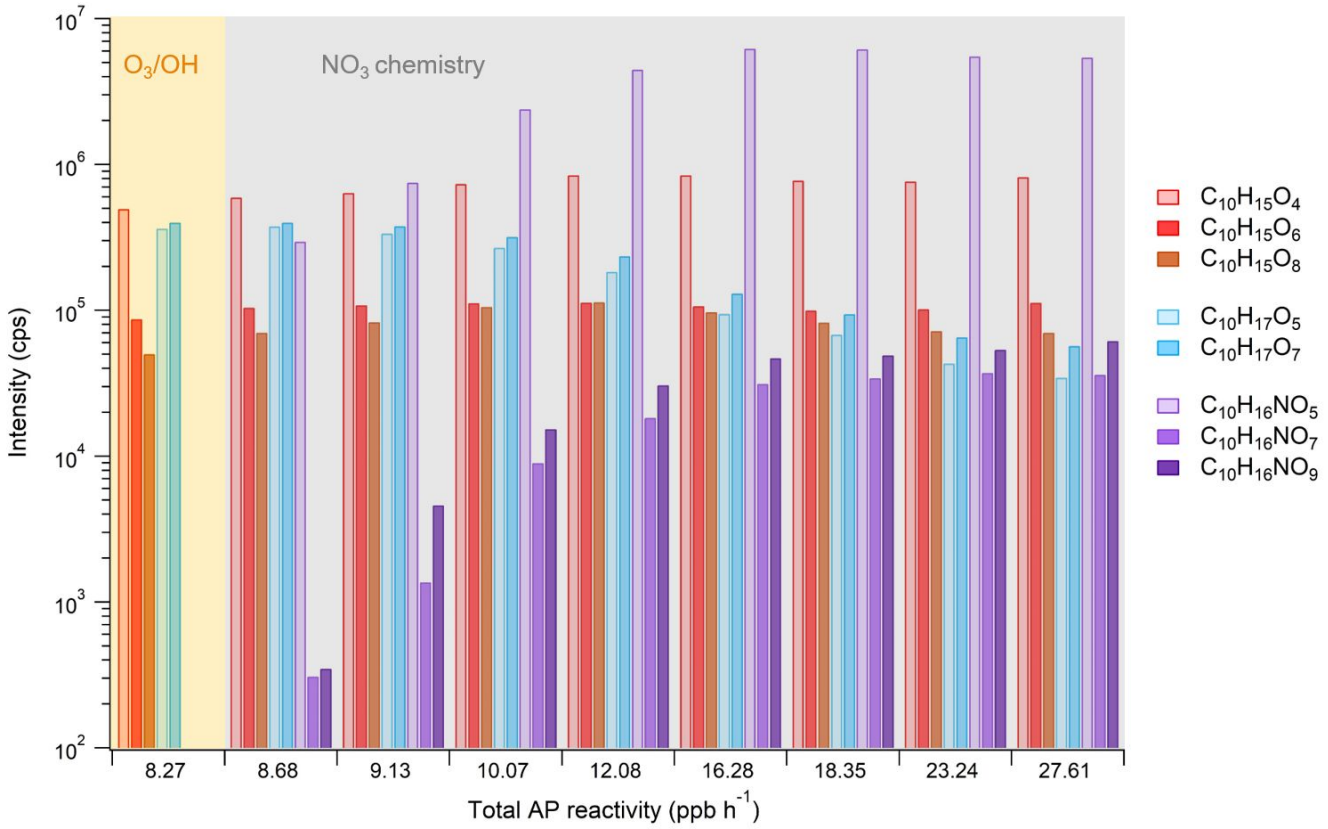

116

117 **Figure S13. Distribution of peroxy radicals measured by CI-(NH_4^+)-Orbitrap in OFR experiments.**

118 Intensity of peroxy radicals $C_{10}H_{15}O_x$ from O_3, $C_{10}H_{17}O_x$ from OH and $C_{10}H_{16}NO_x$ from NO_3 reaction

119 distributed by total α-pinene reactivity. Results from O_3/OH chemistry are shaded in yellow and those

120 from NO_3 chemistry in gray.

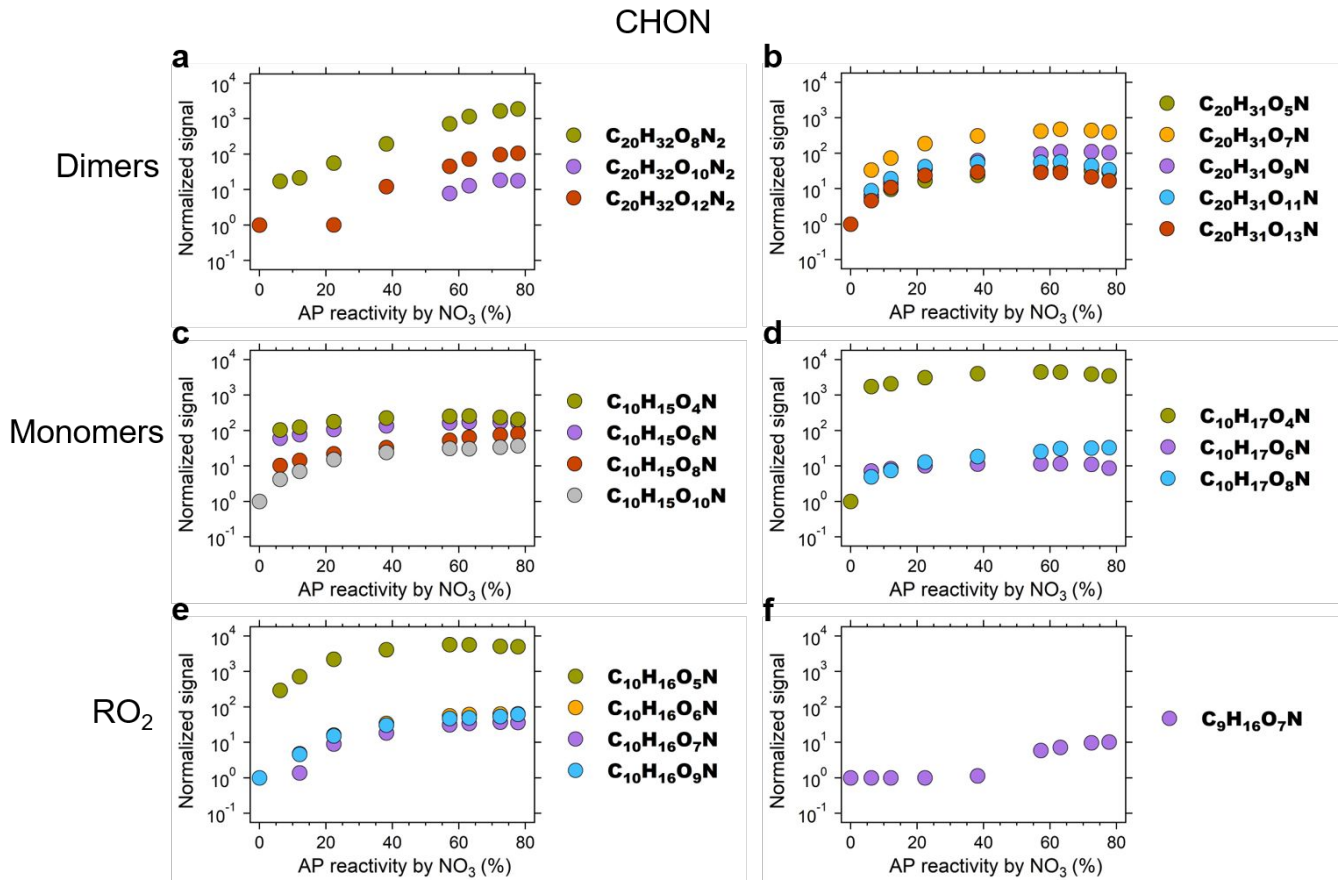

Figure S14. CHON in OFR experiments measured by CI-(NH_4^+)-Orbitrap. Normalized signals of dinitroxy dimers $C_{20}H_{32}O_xN_2$ **(a)** and nitroxy dimers $C_{20}H_{31}O_xN$ **(b)**, organic nitrates $C_{10}H_{15}O_xN$ **(c)** and $C_{10}H_{17}O_xN$ **(d)**, peroxy radicals $C_{10}H_{16}O_xN$ **(e)** and $C_9H_{16}O_xN$ **(f)** derived from NO_3 chemistry as a function of α-pinene reactivity by NO_3 radicals.

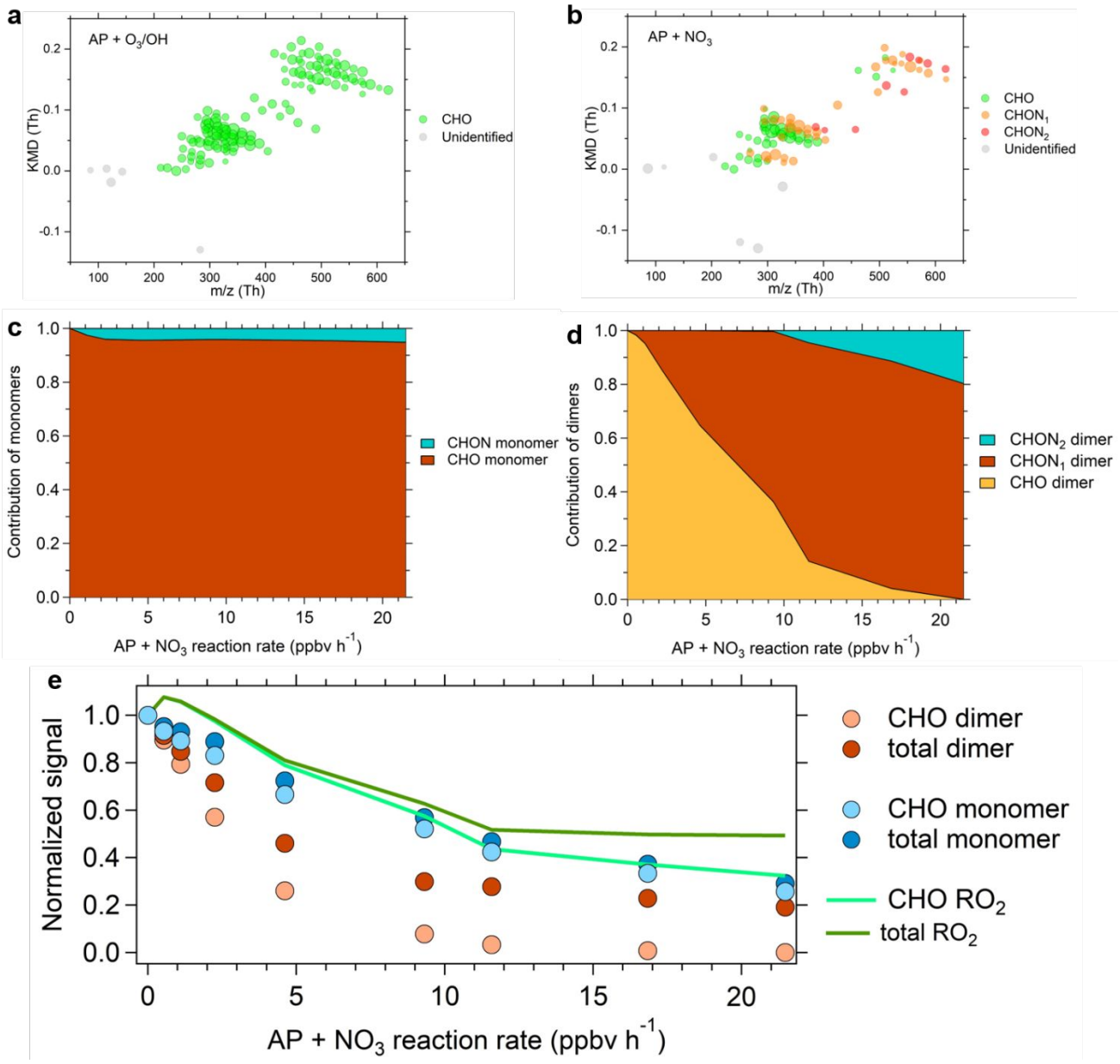

126

127 **Figure S15. Sensitivity of NO_3 radicals to the formation of OVOCs in OFR experiments measured**
128 **by CI-(NO_3^-)-Orbitrap. (a** and **b)** Kendrick mass defect plots of gaseous compounds observed in the
129 reaction of α-pinene with O_3/OH **(a)** and NO_3 radical **(b)**. The circles are the measured ions colored by
130 groups: CHO, $CHON_1$, $CHON_2$, and unidentified compounds, the sizes of which correspond to their
131 logarithmic intensities. The unidentified compounds represent products with apparent evolution but
132 unassigned molecular formulae. **(c** and **d)** Contribution of CHO monomers and CHON monomers to total
133 monomers **(c)**, CHO dimers, $CHON_1$ dimers, and $CHON_2$ dimers to total dimers **(d)** plotted against α-
134 pinene oxidation rate by NO_3 radicals. **(e)** Normalized signals of CHO monomers, CHO dimers, and CHO
135 RO_2 as a function of α-pinene oxidation rate by NO_3 radicals. Ion signals are normalized to the signal in
136 O_3/OH chemistry for comparison.

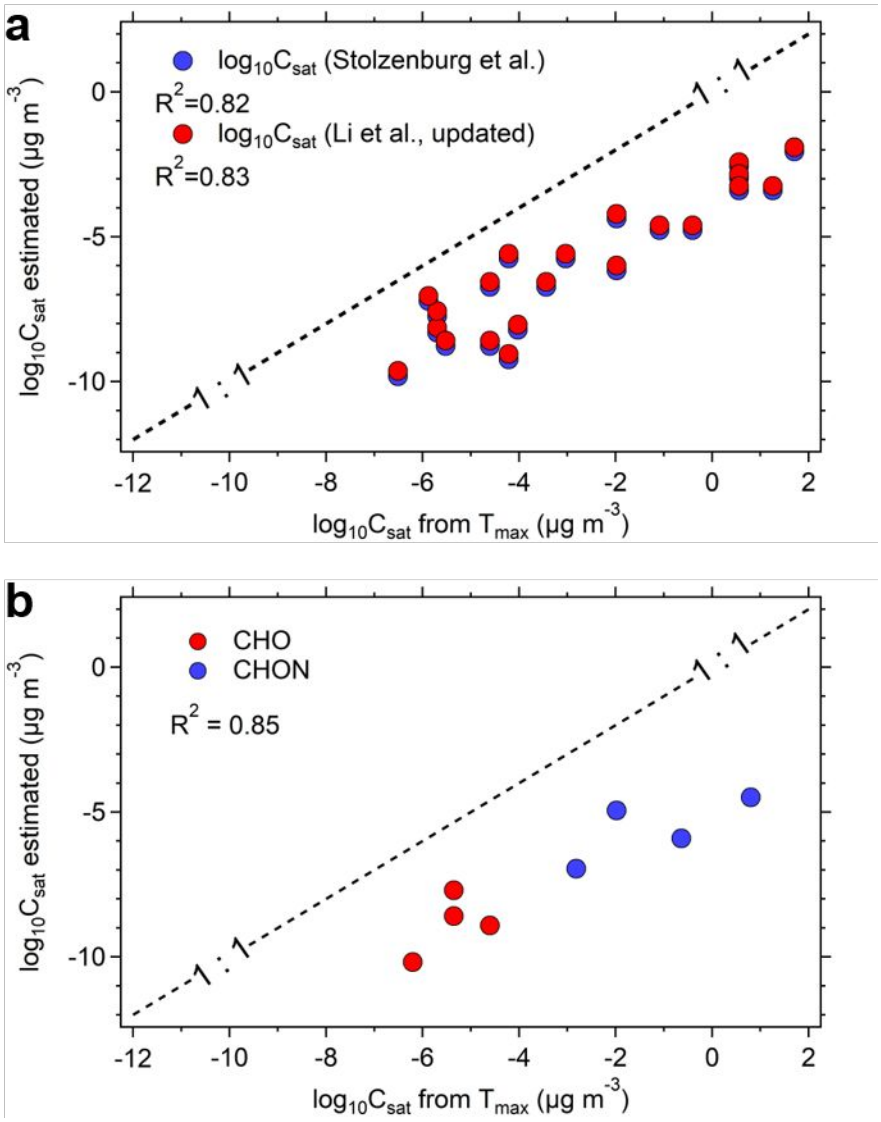

Figure S16. Volatility of CHO in the particle phase measured by FIGAERO-CIMS vs. estimated by the VBS parameterizations in the CLOUD chamber. (a) Saturation vapor concentrations ($\log_{10}C_{sat}$) of CHO species formed from α-pinene ozonolysis in the particle phase are predicted by two parameterizations of Stolzenburg et al.[1] (colored in blue) and Li et al. (updated by Isaacman-VanWertz and Aumont)[2] (colored in red). The measured $\log_{10}C_{sat}$ are calculated using the thermal-desorption volatility calibration curve obtained by calibrants correlating their $\log_{10}C_{sat}$ with $1/T_{max}$ using FIGAERO-CIMS[3]. The gas phase parameterizations are applied assuming compounds with same molecular formulae to have the same structure as in the particle phase. **(b)** Saturation vapor concentrations of selected CHO dimers and CHON dimers in the particle phase measured versus predicted by modified Li et al. approach. A good correlation R^2 of 0.85 validates the consistency between direct FIGAERO volatility measurements and VBS parameterizations.

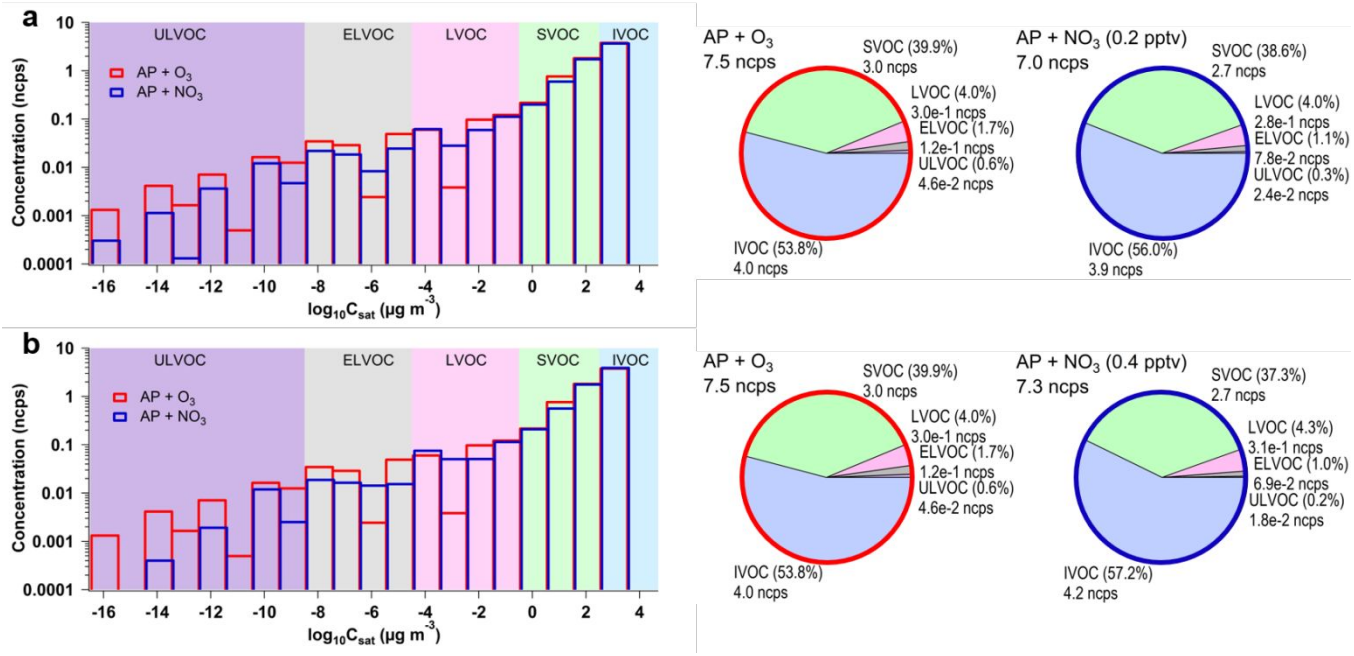

Figure S17. Volatility distribution of OVOCs measured by CI-(NH_4^+)-Orbitrap in the CLOUD chamber. Monomers $C_{9\text{-}10}$ and dimers $C_{18\text{-}20}$ binned to a volatility distribution showing the measured relative abundance in pure O_3 and NO_3 chemistry, respectively; simulated NO_3 concentration was ~0.2 pptv **(a)** and ~0.4 pptv **(b)**. The background colors represent the saturation concentration (C_{sat}) in the range of ultra-low volatility (ULVOCs, purple), extremely low volatility (ELVOCs, gray), low volatility (LVOCs, pink), semi-volatile (SVOCs, green) and intermediate volatility (IVOCs, blue) organic compounds.

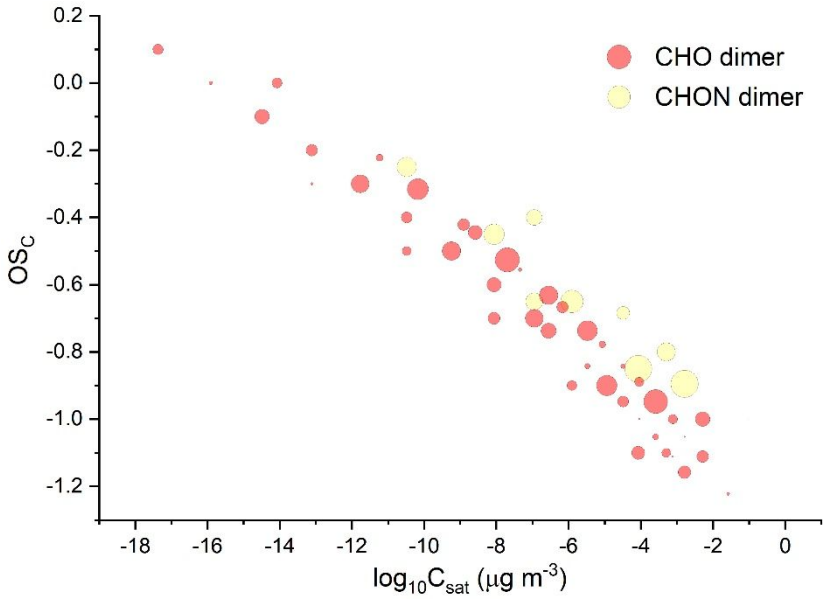

158

159 **Figure S18. Distribution of CHO dimers and CHON dimers measured by CI-(NH_4^+)-Orbitrap in the**
160 **CLOUD chamber plotted on a two-dimensional VBS.** Oxidation state OS_C=2*O/C-H/C. The marker
161 size is scaled by the intensity.

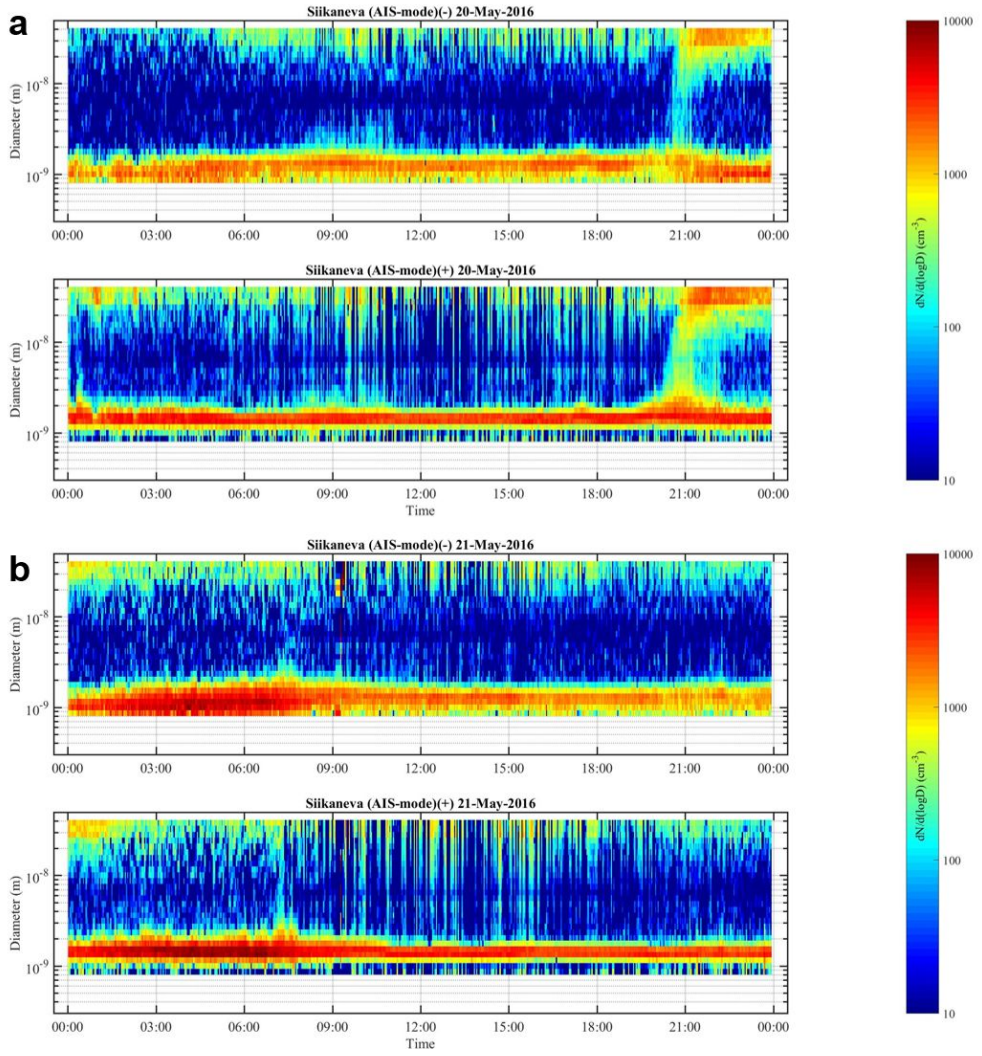

Figure S19. Nocturnal NPF event and nonevent measured by AIS during Siikaneva campaign. Example of a nucleation event **(a)** and non-nucleation event **(b)** at night showing the size evolution of positive and negative ions. The color scale shows the number concentration of ions.

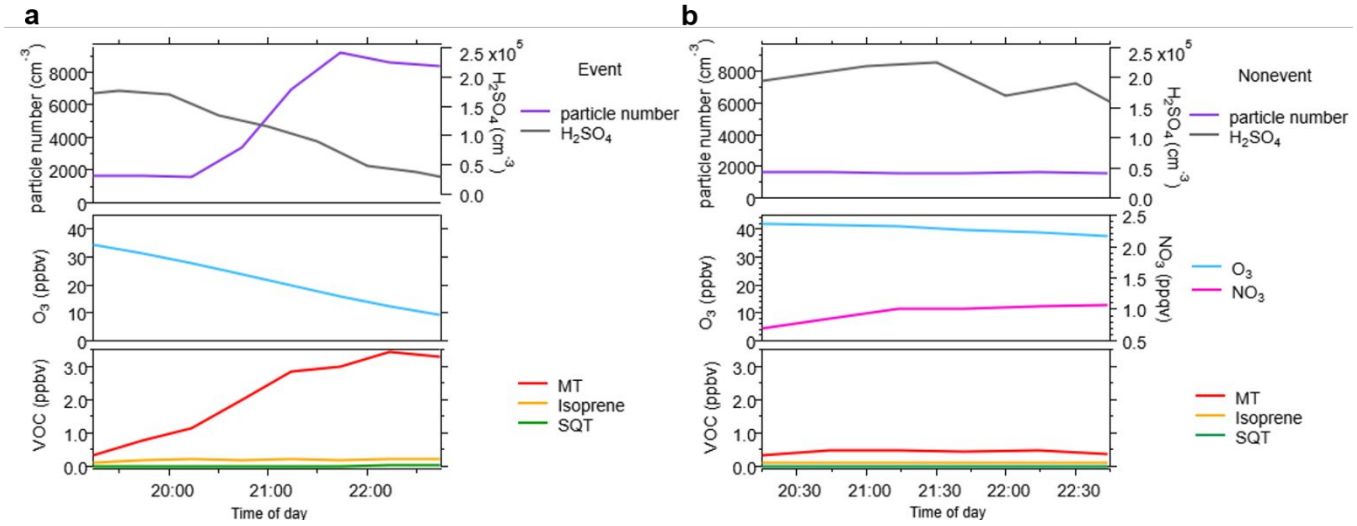

Figure S20. Time evolution of particle number, H_2SO_4, VOC, O_3 and estimated NO_3 in a nocturnal NPF event and nonevent during Siikaneva campaign. (a) Concentration evolution of particle number, H_2SO_4, monoterpene (MT), isoprene, sesquiterpenes (SQT), and O_3 in the NPF event. **(b)** Concentration evolution of particle number, H_2SO_4, monoterpene (MT), isoprene, sesquiterpenes (SQT), O_3 and estimated NO_3 in the non-nucleation event. Unfortunately, NO_x measurement was not available in Siikaneva, in particular for event night with decoupling process. Concentration of NO_3 in nonevent (no decoupling process occurred) was estimated from the NO_x concentration measured at Hyytiälä in a boreal forest, ~5 km east of Siikaneva.

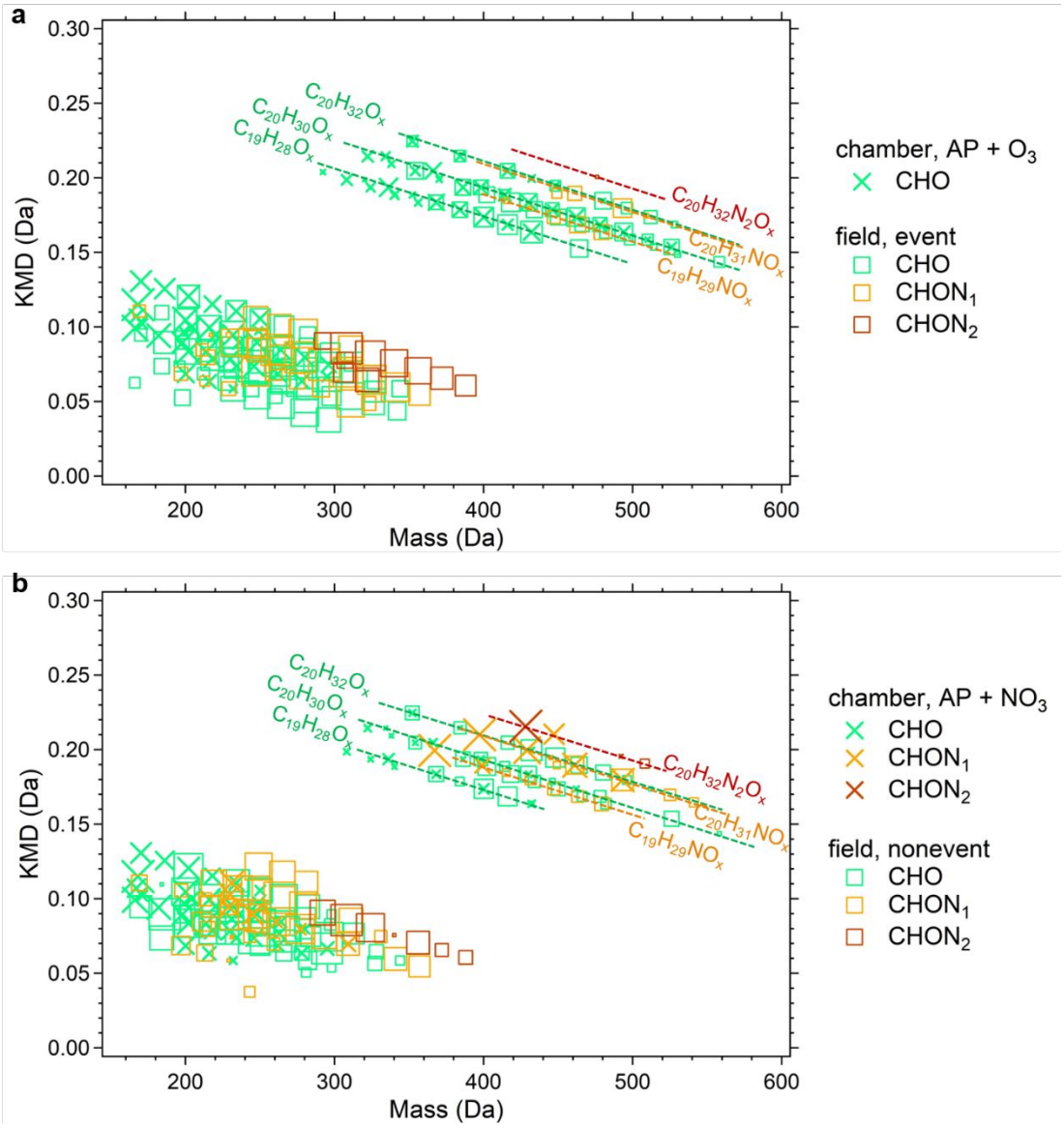

Figure S21. Kendrick mass defect plots of oxygenated compounds observed in the CLOUD chamber and wetland. Mass defect plots for $C_{9\text{-}10}$ monomers and $C_{19\text{-}20}$ dimers in O_3 stage of chamber versus a nocturnal NPF event **(a)** and in NO_3 stage of chamber versus a nonevent **(b)**. The circles are the measured molecules colored by groups: CHO, $CHON_1$, and $CHON_2$, the sizes of which correspond to their logarithmic intensities. Cross and square markers correspond to chamber and campaign data measured by CI-(NH_4^+)-Orbitrap and CI-(NO_3^-)-APi-TOF, respectively. The abscissa represents the measured mass of the compounds which has subtracted the reagent ions.

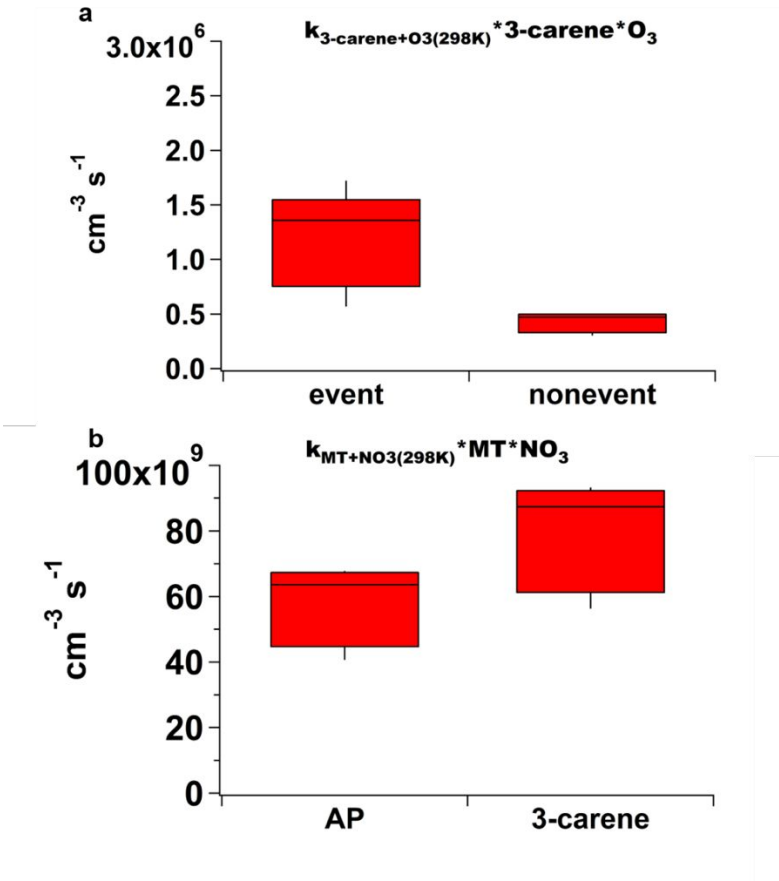

Figure S22. Monoterpene reaction rate in a nocturnal NPF event and nonevent during Siikaneva campaign. (a) Ozonolysis rate of Δ^3-carene in the NPF event and nonevent. **(b)** Reactivity of α-pinene and Δ^3-carene by NO_3 radical in the nonevent. Concentration of monoterpenes were measured, but the composition could not be classified due to the instrumental limitation during the campaign. α-Pinene is the most abundant monoterpene in May at Hyytiälä, followed by Δ^3-carene[4]. Hence, reactivities of α-pinene and Δ^3-carene are calculated and represent the reactivity range by assuming the total monoterpene concentration is that of one monoterpene. The reaction rate of these monoterpenes with estimated NO_3 radical in the nonevent are also assessed at 298 K, given that the most reaction rate constants are only available at room temperature from International Union of Pure and Applied Chemistry (IUPAC, https://iupac.aeris-data.fr/en/home/). Considering the Δ^3-carene concentration being a factor of ~2 lower than that of α-pinene[4], the dominating monoterpene reactivity by O_3 and by NO_3 radical in Siikaneva are both from α-pinene.

Supplementary References

1 Stolzenburg, D. *et al.* Rapid growth of organic aerosol nanoparticles over a wide tropospheric temperature range. *Proceedings of the National Academy of Sciences* **115**, 9122-9127 (2018). https://doi.org:doi:10.1073/pnas.1807604115

2 Isaacman-VanWertz, G. & Aumont, B. Impact of organic molecular structure on the estimation of atmospherically relevant physicochemical parameters. *Atmospheric Chemistry and Physics* **21**, 6541-6563 (2021). https://doi.org:10.5194/acp-21-6541-2021

3 Wang, M. *et al.* Photo-oxidation of Aromatic Hydrocarbons Produces Low-Volatility Organic Compounds. *Environmental science & technology* **54**, 7911-7921 (2020). https://doi.org:10.1021/acs.est.0c02100

4 Vettikkat, L. *et al.* High emission rates and strong temperature response make boreal wetlands a large source of isoprene and terpenes. *Atmospheric Chemistry and Physics* **23**, 2683-2698 (2023). https://doi.org:10.5194/acp-23-2683-2023